Restricted Rotational Flexibility of the C5α-Methyl-Substituted Carbapenem NA-1-157 Leads to Potent Inhibition of the GES-5 Carbapenemase

Nichole K. Stewart[1], Marta Toth[1], Pojun Quan[2], Michael Beer[3,4], John D. Buynak[2*], Clyde A. Smith[5,6*], and Sergei B. Vakulenko[1*]

[1] Department of Chemistry and Biochemistry, University of Notre Dame, Notre Dame, IN 46556, USA

[2] Department of Chemistry, Southern Methodist University, Dallas, TX 75275, USA

[3] School of Cellular and Molecular Medicine, University of Bristol, Bristol, United Kingdom

[4] Centre for Computational Chemistry, School of Chemistry, University of Bristol, Bristol, United Kingdom

[5] Stanford Synchrotron Radiation Lightsource, Stanford University, Menlo Park, CA 94025, USA

[6] Department of Chemistry, Stanford University, Stanford, CA 94305, USA

[*] To whom correspondence should be addressed:

Prof. Sergei B. Vakulenko, ph: 574-631-2935, Fax: 574-631-6652, E-mail: svakulen@nd.edu

Dr. Clyde A. Smith, ph: 650-926-8544, Fax: 650-926-3292, E-mail: csmith@slac.stanford.edu

Prof. John D. Buynak, ph: 214-768-2484, Fax: 214-768-4089, E-mail: jbuynak@smu.edu

ABSTRACT

Carbapenem antibiotics are used as a last-resort treatment for infections caused by multidrug-resistant bacteria. The wide spread of carbapenemases in Gram-negative bacteria has severely compromised the utility of these drugs and represents a serious public health threat. To combat carbapenemase-mediated resistance, new antimicrobials and inhibitors of these enzymes are urgently needed. Here we describe interaction of the atypically C5α-methyl-substituted carbapenem, NA-1-157, with the GES-5 carbapenemase. MICs of this compound against *Escherichia coli*, *Klebsiella pneumoniae*, and *Acinetobacter baumannii* producing the enzyme were reduced 4-16-fold when compared to MICs of the commercial carbapenems, reaching clinically sensitive breakpoints. When NA-1-157 was combined with meropenem, a strong synergistic effect was observed. Kinetic and ESI-LC/MS studies demonstrated that NA-1-157 is a potent inhibitor of GES-5, with a high inactivation efficiency of $(2.9 \pm 0.9) \times 10^5$ $M^{-1}s^{-1}$. Acylation of GES-5 by NA-1-157 is biphasic, with the fast phase completing within seconds, and the slow phase taking several hours and likely proceeding through a reversible tetrahedral intermediate. Deacylation was extremely slow ($k_3 = (2.4 \pm 0.3) \times 10^{-7}$ s^{-1}), resulting in a residence time of 48 ± 6 days. MD simulation of the GES-5-meropenem and GES-5-NA-1-157 acyl-enzyme complexes revealed that the C5α-methyl group in NA-1-157 sterically restricts rotation of the 6α-hydroxyethyl group preventing ingress of the deacylating water into the vicinity of the scissile bond of the acyl-enzyme intermediate. These data demonstrate that NA-1-157 is a potent irreversible inhibitor of the GES-5 carbapenemase.

KEYWORDS. Carbapenemase, carbapenem, inhibitor, crystal structure, antibiotic resistance, kinetics

Dissemination of carbapenem-resistant Gram-negative bacteria has significantly exacerbated the worldwide problem of antibiotic resistance. Though several mechanisms can contribute to carbapenem resistance, such as reduced permeability, upregulated efflux, and modification of the drug target, the penicillin-binding proteins (PBPs), the most prevalent mechanism is production of carbapenemases, enzymes that hydrolyze carbapenem antibiotics, thus rendering them inactive.[1] Carbapenems belong to the largest family of antibiotics, β-lactams, and are often used as last-resort therapy for deadly infections caused by multidrug-resistant bacterial pathogens.[2] As such, spread of carbapenemase-producing bacteria is especially worrisome as it further narrows already limited therapeutic options.

Carbapenemases are divided into four molecular classes, with classes A, C, and D utilizing an active-site serine for catalysis, whereas those from class B are zinc metalloenzymes. Of these, the class A enzymes include most of the clinically-relevant carbapenemases, such as those from the GES, KPC, SME, FRI, and IMI/NMC-A families, and the CTX-M-33, SHV-38, and PenA enzymes.[3-4] Sometimes referred to as "minor carbapenemases", the GES-type enzymes are becoming more frequently identified in Gram-negative clinical isolates. Originally, they were mainly found in *Pseudomonas aeruginosa*[5], however, more recently they have disseminated to various members of the *Enterobacterales* order, such as *Klebsiella pneumoniae, Escherichia coli,* and *Enterobacter cloacae,* and also *Acinetobacter baumannii*.[3] This constitutes a troubling trend that highlights potential of these enzymes to become one of the major carbapenemases. The first GES variant, GES-1, was isolated from *K. pneumoniae* in 1998 and possessed extended-spectrum activity against β-lactams, including penicillins and broad-spectrum cephalosporins, but not carbapenems or cephamycins.[6] However, since then nearly 60 variants have been detected worldwide, with 33 of them having the Gly170Ser mutation, which is associated with resistance to carbapenems in clinical isolates.[7] Infections caused by *P. aeruginosa* expressing such enzymes are associated with higher mortality rates.[8] In some cases, multiple GES variants have been found in the same

isolate.[9-11] Additionally, two different GES enzymes were found to express in tandem in two *P. aeruginosa* isolates, and it was suggested that they produce a synergistic effect that leads to high-levels of resistance to β-lactams.[12] GES variants have also been identified in combination with other carbapenemases, such as the class B metalloenzymes VIM-11 and IMP-1 and the class D enzyme OXA-23, extending the spectrum of β-lactam resistance and increase of its levels.[10, 13-14] These findings further underscore the clinical importance of GES-type enzymes and the need for novel antimicrobial agents to fight GES-mediated β-lactam resistance.

One successful strategy for circumventing antibiotic resistance is use of β-lactamase inhibitors in combination with β-lactam antibiotics. The earliest clinically used inhibitors active against class A enzymes, clavulanic acid, tazobactam, and sulbactam, were successfully used to treat infections caused by bacteria producing narrow spectrum β-lactamases.[15] However, emergence of inhibitor-resistance and pathogens producing extended spectrum β-lactamases significantly diminished the therapeutic utility of classical β-lactamase inhibitor/β-lactam combinations. As a result, modified β-lactam-based inhibitors (e.g. enmetazobactam), and also non-β-lactam inhibitors, such as the diazabicyclooctanes (DBOs) and boronates, were developed.[16] These inhibitors vary in their spectrum of activity and mode of inhibition, and several of them are approved for clinical use to treat infections caused by some carbapenemase-producing pathogens.[17-20] Another obvious, but less exploited strategy to fight carbapenemase-mediated resistance, is to modify carbapenem antibiotics themselves, to render them resistant to degradation by these enzymes, as these drugs are well studied, widely used, and have a wide spectrum of activity, very low toxicity, and well-known pharmacological properties. In one of the earlier studies, several carbapenem derivatives with a C5α-methyl group substitution were synthesized, and some of them demonstrated good activity mostly against Gram-positive bacteria.[21] Using quantum mechanical/molecular mechanical-based molecular dynamics (MD) simulations, it was shown that the C4-methyl group of aztreonam is responsible

for the slower deacylation rate of this monobactam from a class C β-lactamase relative to the cephalosporin cephalothin.[22]

More recently, it was reported that the C5α-methyl group-containing, novel carbapenem NA-1-157 (Figure 1A) exhibits potent activity against the important clinical pathogens, *Mycobacterial tuberculosis* and *Mycobacterial abscessus*[23], and *Enterobacterales* producing the major class D carbapenemase OXA-48[24]. Upon further evaluation of this drug, we observed that NA-1-157 also possesses potent activity against bacteria producing the GES-5 carbapenemase. Here we report the microbiological, biochemical, and structural characterization of NA-1-157 with GES-5 and show it is a potent inhibitor of the enzyme.

RESULTS AND DISCUSSION

Antimicrobial Susceptibility Testing. Since the GES-5 carbapenemase is commonly found in bacteria from the *Enterobacterales* order, we evaluated the activity of NA-1-157 by measuring its MICs against *E. coli* JM83 and *K. pneumoniae* ATCC 13883 expressing the enzyme. We observed that the compound demonstrated 4-fold more potent antimicrobial activity than meropenem, where its MICs was 0.5 μg/mL against both bacteria, which is below the clinically susceptible level (1 μg/mL) as defined by the Clinical Laboratory Standards Institute (CLSI)[25] (Table 1). Next, we assessed the MICs of meropenem in combination with NA-1-157 by performing a checkerboard assay. When the compound was added at a concentration 2-fold below its MIC, the MICs of meropenem were reduced 64-fold to the background level of each strain (0.031 μg/mL). When NA-1-157 was added at a lower concentration (8-fold below its MIC), the MICs of meropenem were still reduced below the clinically sensitive level to 0.5 μg/mL for both strains. The heat maps generated from the checkerboard data are shown in Figure S1. To quantify the interaction between meropenem and NA-1-157, we calculated the fractional inhibitory concentration (FIC) index, where values <0.5 indicate synergy.[26] For *E. coli* JM83 and *K. pneumoniae* ATCC 13883

expressing GES-5, the FIC index values were 0.31 and 0.19 (in both cases with 0.125 μg/mL meropenem and NA-1-157), respectively, showing that there is a synergistic relationship between the two carbapenems for both bacteria. We also evaluated the activity of NA-1-157 against the important clinical pathogen *A. baumannii* expressing the enzyme from a shuttle vector[27]. The MICs of meropenem and imipenem against this strain were 32 and 16 μg/mL, respectively, while the MIC of NA-1-157 was just 2 μg/mL, which is at the clinically susceptible level[25] (Table 2). Also of note, the MIC of the compound against the parental sensitive *A. baumannii* strain was the same as that of meropenem, suggesting that structural changes in NA-1-157 do not affect its permeability and/or binding to PBPs in this bacterium. Together, these results demonstrate that NA-1-157 is either an inhibitor or a very poor substrate of GES-5 and indicate that the compound could potentially be used alone as an antibiotic or as an inhibitor in combination with current commercial antibiotics against bacteria expressing this carbapenemase.

Enzyme Kinetics. Next, we performed detailed kinetic studies to investigate the mechanism of interaction between NA-1-157 and GES-5. To evaluate whether there was any reaction between them, we monitored the change in absorbance at 298 nm under steady-state conditions with an excess of the compound. The progress curves showed that there was a decrease in absorbance, indicating opening of the β-lactam ring of NA-1-157 and acylation of GES-5, where the velocity progressively slowed over the course of several hours, at which point the reaction had ceased (representative curve shown in Figure 2A). This measurement also showed that the initial absorbance was lower than expected for the concentration of the compound used, and the total change in absorbance observed over the course of the reaction was about 2-fold lower than the concentration of GES-5. These data indicated that the reaction was biphasic, where the fast initial phase took place during the manual mixing time of the experiment. To test this, we measured the reaction using a stopped-flow instrument and found that there was indeed a fast phase of the reaction

that was complete within a second (Figure 2A insert) as has been observed with some commercial carbapenems and class A and D enzymes.[28-31] The total change in absorbance for both the fast and slow reactions was close to the concentration of GES-5, with the slow and fast phases corresponding to 55 ± 8% and 56 ± 9%, respectively, demonstrating that no detectible deacylation took place during the 5 h reaction.

To evaluate the rate constants $k_{2\ fast}$ and $k_{2\ slow}$ (Scheme 1), corresponding to the fast and slow phases of the acylation reaction, respectively, we performed single-turnover experiments with a molar excess of GES-5 over NA-1-157. For the fast phase, the reaction comprised 46 ± 5% of the total, and the acylation rate constant $k_{2\ fast}$ was calculated to be 99 ± 31 s^{-1} (Table 3 and Figure 2B). This value is similar to the lower limit of $k_{2\ fast}$ determined for the acylation of GES-5 by the closest structural analogue of NA-1-157, meropenem, and at least 4.5-fold slower than that of imipenem.[29] For the slow phase that comprised 47 ± 2% of the total reaction, saturation was reached with the lowest enzyme concentration used (5-fold molar excess over NA-1-157), and the $k_{2\ slow}$ value ((2.6 ± 0.1) × 10^{-4} s^{-1}) was nearly 400,000-fold lower than that of $k_{2\ fast}$ (Table 3 and Figure 2C). This $k_{2\ slow}$ value is 330- and 1300-fold lower than that measured for meropenem and imipenem, respectively. Combined, these data demonstrate that structural differences between NA-1-157 and the other carbapenems mostly impact the slow phase of acylation.

Next, we evaluated whether NA-1-157 is able to deacylate from GES-5 by performing jump dilution experiments after overnight preincubation to ensure that all enzyme molecules were in the covalent complex. Following jump dilution, we observed return of only a tiny fraction (<1% after 2 h) of enzyme activity using a continuous absorbance assay (Figure 2D). Subsequently, we used a discontinuous assay to monitor restoration of enzyme activity for up to 30 days (the control showed that during this time the enzyme retained >80% activity). Based on these data, we calculated the rate constant for deacylation, k_3

(Scheme 1), to be $(2.4 \pm 0.3) \times 10^{-7}$ s^{-1}, which translates to a residence time of 48 ± 6 days (Table 3); this shows that for clinical purposes, NA-1-157 is an irreversible covalent inhibitor of GES-5.

To get further insights into the mechanism of inhibition of GES-5 by NA-1-157, we evaluated steady-state inactivation kinetic parameters by performing a competition experiment using the chromogenic cephalosporin nitrocefin as a reporter substrate. In this experiment, the progress curves for hydrolysis of nitrocefin showed a slow onset of inhibition, which is typically observed for slow binding inhibitors.[32] Inhibition by slow binding inhibitors can proceed through either a one-step or a two-step mechanism. For a one-step mechanism, the relationship between k_{inter} (k_{inter} is the apparent first-order rate constant for interconversion between the initial and steady-state velocities of nitrocefin hydrolysis) and inhibitor concentration is linear, whereas for a two-step mechanism, the relationship can be either hyperbolic or linear.[33-34] From the progress curves, the k_{inter} values were evaluated for various concentrations of NA-1-157 (up to the detection limit of the assay; plot is shown in Figure 2E). Under these conditions, it was not clear whether the generated curve is linear or hyperbolic. Because it is generally accepted that β-lactamase-carbapenem chemistry proceeds through a two-step mechanism, we used this model to analyze our inactivation data. In this mechanism, there is an initial binding event to form the noncovalent Michaelis complex that proceeds through a tetrahedral intermediate transition state to form the covalent acyl enzyme.[15]

First, we evaluated which steps in the catalytic mechanism of inhibition of GES-5 by NA-1-157 could contribute to the inactivation process. The progress curves for nitrocefin hydrolysis by GES-5 in the presence of NA-1-157 showed the enzyme was inactivated in less than 2 min (data not shown). This shows that only the fast phase of acylation of GES-5 by NA-1-157 (described by $k_{2\ fast}$), which completes within seconds, contributes to the inactivation process, and excludes the contribution of the slow phase that takes several hours. However, the fast phase comprised only about half of the total acylation reaction, indicating

that there must be another contributing factor to inactivation of GES-5. To investigate this, we performed the jump dilution experiment after a short preincubation time (20 s) to allow for only the fast phase of acylation to occur, and saw that approximately 44% of GES-5 activity returned (Figure 2F). This result is in agreement with our single-turnover data showing that around half of the enzyme population acylates fast according to the $k_{2\ fast}$ rate constant (Table 3), and demonstrates that during this short time, only part of the GES-5 molecules form the irreversible covalent acyl-enzyme intermediate, while the remaining molecules must form a reversible complex. The progress curves for nitrocefin hydrolysis by GES-5 in the presence of NA-1-157 also support that inactivation is at least partly reversible, as the steady-state velocities never dropped to zero. Together, these results suggest that inactivation of GES-5 by NA-1-157 results from simultaneous formation of both the covalent irreversible acyl-enzyme intermediate formed during the fast phase of acylation and a reversible species. To evaluate the inactivation kinetics, we determined the maximum rate of inactivation of GES-5 by NA-1-157. Commonly, this is often reported in the literature as k_{inact}, which describes inhibition resulting from formation of only irreversible species.[32] However, since inactivation of GES-5 by NA-1-157 results from formation of both irreversible and reversible species, we call this parameter $k_{NA\text{-}1\text{-}157}$, similar to what was reported for inactivation of GES-1, GES-2, and GES-5 by clavulanic acid and GES-2 by tazobactam.[35-36] We also evaluated K_I, which is the concentration of NA-1-157 required to reach one half of $k_{NA\text{-}1\text{-}157}$. From fitting the data (Figure 2E), the parameters $k_{NA\text{-}1\text{-}157}$ and K_I were calculated to be 4.1 ± 0.8 s^{-1} and 14 ± 3 μM, respectively, which shows that NA-1-157 has a relatively high inactivation efficiency ($k_{NA\text{-}1\text{-}157}/K_I = (2.9 \pm 0.9) \times 10^5\ M^{-1}s^{-1}$) and is a potent inhibitor of GES-5.

To investigate further whether inactivation of GES-5 by NA-1-157 results from formation of both the irreversible acyl-enzyme intermediate and a reversible complex, we analyzed the enzyme species present in the reaction at different time points using electrospray ionization-liquid chromatography/mass

spectrometry (ESI-LC/MS) under denaturing conditions. For this experiment, the enzyme was incubated with excess NA-1-157, and aliquots were removed at predetermined time points. ESI-LC/MS analysis of these samples revealed that already at the earliest time point (20 s), nearly all (96%) GES-5 was in a covalent complex with NA-1-157 (29,629 Da), as judged by the increase in mass of the apo enzyme of 384 Da (Figure S2A). At later time points in the experiment (1 h), we also observed two other species that were 142 and 158 Da smaller than the parent species (29,487 and 29,471 Da; data not shown). We believe that these smaller species are the result of fragmentation of NA-1-157 due to the ESI-LC/MS conditions, similar as has been reported for meropenem[37-38]. This result is not in agreement with our kinetic data (described above) showing that during the time scale of 20 s, only half of the GES-5 molecules form the irreversible covalent acyl-enzyme intermediate, while the remaining molecules form a reversible complex. Such reversible covalent complex may be represented by a tetrahedral intermediate (oxyanion) as has been described for the interaction of Ldt_{fm} with β-lactams,[39] but, to our knowledge, has not been reported for β-lactamases. To confirm whether any of the observed covalent GES-5-NA-1-157 species is indeed reversible, we repeated the experiment with some modifications. As before, GES-5 was incubated with an excess of NA-1-157, aliquots were taken at three time points (2 min, 30 min, and 2 h), and excess compound was rapidly removed chromatographically. Subsequently, another carbapenem, NA-1-208[23] (Figure 1A), which has a molecular mass 14 Da larger than NA-1-157 and forms a stable acyl-enzyme complex with GES-5 (Figure S2B), was added in a large excess and incubated for 30 min prior to analysis. ESI-LC/MS measurements of these samples revealed the presence of two different covalent species with masses corresponding to the GES-5-NA-1-157 and GES-5-NA-1-208 complexes (Figure S2C). The relative abundances of these species were 54 ± 11% and 47 ± 11% after 2 min and 70 ± 12% and 30 ± 12% after 30 min for the GES-5-NA-1-157 and GES-5-NA-1-208 complexes, respectively, while after 2 h only the GES-5-NA-1-157 covalent complex was observed. In all cases, there was no apo enzyme

observed. These results are in agreement with our kinetic data showing that only half of the inhibited enzyme species are represented by a classical acyl-enzyme intermediate, while the remaining is reversible, and requires more than 2 h to eventually convert to the irreversible classical acyl-enzyme intermediate.

Molecular Docking. In order to gain insights into the biphasic acylation observed for the interaction of NA-1-157 with GES-5, molecular docking of intact (non-hydrolyzed) meropenem and NA-1-157 into the apo-GES-5 structure was performed to generate pre-transition state Michaelis models. The binding energies for meropenem and NA-1-157, estimated by ICM-Pro[40], were -9.4 kcal mol^{-1} and -8.4 kcal mol^{-1}, respectively (Table S1), suggesting that GES-5 has an approximately 6-fold lower affinity for NA-1-157 compared to meropenem. The lowest energy poses from multiple docking simulations for both meropenem and NA-1-157 had the molecules in similar conformations, with the β-lactam ring adjacent to the catalytic serine and the C3 carboxylate group interacting with three conserved residues, Thr235, Thr237, and Arg244 (Figures 3A and 3B). The O7 carbonyl on the β-lactam ring was positioned in the vicinity of the oxyanion hole, a well-characterized feature of the serine β-lactamases[41], where it accepts a hydrogen bond from the main chain amide nitrogen atom of Thr237. The site of nucleophilic attack (the C7 carbon atom) is 2.99 Å and 2.91 Å from the Oγ atom of the catalytic Ser70 in the GES-5-meropenem and GES-5-NA-1-157 models, respectively.

Superposition of the GES-5-meropenem and GES-5-NA-1-157 Michaelis complexes (Figure 3C) shows that the C7-O7 carbonyl atoms and the C3 carboxylate groups overlap almost perfectly even though the β-lactam ring and the fused pyrroline rings are slightly twisted in one complex relative to the other. This in turn displaces the sulfur atom and the pyrrolidine rings by approximately 0.5 Å. In both molecules, the 6α-hydroxyethyl (6α-HE) group is in an outward-facing orientation (relative to the catalytic serine and

lysine residues) (Figures 3A and 3B). A hydrogen bond between the O62 atom and the Nδ2 atom of Asn132 anchors the 6α-HE group in this rotamer conformation.

To evaluate whether these models are viable Michaelis complexes, we compared them to known Michaelis complexes of β-lactam antibiotics with class A β-lactamases (BlaC from *Mycobacterium tuberculosis*, PDB codes 3NY4, 7K8F, and 7K8H, and SFC-1 from *Serratia fonticola*, PDB code 4EUZ). The orientation and interactions of the β-lactams with these enzymes (namely the C7-Oγ(Ser70) distances and the angle between the plane of the β-lactam ring and the Oγ) are almost identical to the those seen in our GES-5 models, suggesting that meropenem and NA-1-157 in these models are properly positioned for efficient attack by the catalytic serine.

Our kinetic studies showed that GES-5 acylation by meropenem and NA-1-157 proceeds through two phases, fast and slow. The fast phase for both carbapenems completes within seconds, and the $k_{2\ fast}$ values are very similar. This is reflected in the docking studies that showed that the initial orientations with respect to the catalytic serine are almost identical (Figure 3C). Unlike the fast phase, the slow phases of enzyme acylation are very different. For meropenem, this phase is complete in around 40 s[29], whereas for NA-1-157, it requires several hours to complete. Using MS experiments we observed that during the slow phase, a non-classical covalent interaction (which we surmise could be a tetrahedral transition state) between GES-5 and NA-1-157 forms, which very slowly gets converted into the acyl enzyme. The subsequent MS competition experiment showed that this interaction is reversible, where at the earliest time point NA-1-208 substituted NA-1-157 in the GES-5 active site. This implies that NA-1-157 must leave the active site, which is then occupied by the competing carbapenem. To see whether we could observe this reversibility, MD simulations were performed on the GES-5-NA-1-157 and GES-5-meropenem Michaelis models. The root-mean-square deviations (*rmsd*s) of the protein main chain relative to the initial models (1.23 Å for meropenem and 1.26 Å for NA-1-157) showed that in both complexes

the protein remains in a stable conformation (Figure 4A) throughout the entire 100 ns. The *rmsd*s of meropenem relative to its initial position at $t = 0$ ns indicate that the molecule remains close to its docked pose (average *rmsd* of 3.5 Å) (Figure 4B). Visual inspection of the MD trajectory for the GES-5-meropenem Michaelis complex (Supplemental Movie File 1) shows that the core of the molecule remains essentially immobile, and it is rotation of the pyrrolidine-dimethylcarbamoyl tail that predominates in the calculated *rmsd*. This indicates that the GES-5-meropenem Michaelis complex remains viable over the duration of the 100 ns simulation. Conversely, after approximately 35 ns, the NA-1-157 molecule moves to an intermediate position (stage 2) which is on average about 7-8 Å from the initial position (stage 1), and then at around 80 ns, it moves even further to a position (stage 3) approximately 15 Å away (Figure 4B and Supplemental Movie File 2). Examining the interactions between NA-1-157 and the enzyme more closely shows that the O7-N(Thr237) hydrogen bond (Figure 4C; green trace) remains essentially intact through the first 20-25 ns of stage 1, and the C7-Oγ(Ser70) distance (Figure 4C; orange trace) is such that the carbapenem remains positioned for nucleophilic attack. Near the end of stage 1 there is a gradual increase in both interactions leading into the transition to stage 2 at approximately 35 ns. An expanded view of the first 6 ns of stage 1 shows that during the first 2 ns, the C7 atom remains close to the Ser70 side chain (< 3.6 Å) (Figure 4D; orange trace) at a distance favorable for efficient nucleophilic attack, and this may correspond to the initial fast phase of acylation. After 2 ns, the C7-Oγ(Ser70) and O7-N(Thr237) distances slightly lengthen (to ≥ 4 Å and 3.5 Å, respectively) and then remain essentially stable up to approximately 25 ns, after which the GES-5-NA-1-157 Michaelis complex breaks down to a point where nucleophilic attack on the C7 carbon by the catalytic serine would become unfavored. In stage 2, between 35-80 ns, the O7-N(Thr237) bond is fully broken, with an average distance of ~10 Å (Figure 4C; green trace), and the C7 atom is approximately 9 Å from the catalytic serine Oγ, on average (Figure 4C; orange trace). Conversely, the interactions made from the NA-1-157 C3 carboxylate to the side chains of Thr235

(Figure 4E; gray trace), Thr237 (Figure 4E; yellow trace) and Arg244 (Figure 4E; blue trace) remain present throughout both stages 1 and 2 up to ~80 ns. During stage 2 of the simulation, the NA-1-157 molecule pivots in the active site such that the β-lactam ring moves away from the catalytic serine yet retains the C3 carboxylate interactions (Figure 4F). In the final stage, from 80-100 ns, NA-1-157 leaves the active site and resides in the milieu (Figure S3), allowing ingress of a new NA-1-157 molecule into the active site.

Combined, the kinetic, MS, and MD results show that the putative meropenem-GES-5 and NA-1-157-GES-5 Michaelis complexes behave completely differently. Meropenem is retained in the active site and positioned for efficient acylation. NA-1-157 is initially (for the first 2 ns) also positioned for efficient acylation, which occurs only during the fast phase of the reaction. MS experiments showed that during the subsequent slow reversible phase of the reaction, NA-1-157 leaves the active site, which is consistent with the results of the MD simulation and the lower estimated binding affinity compared to meropenem.

The Acyl-Enzyme Structures. The 3D structures of the acyl-enzyme complexes of GES-5-meropenem and GES-5-NA-1-157 were determined by X-ray crystallography. Inspection of the residual electron density in the active site showed that both meropenem and NA-1-157 were clearly present from the t = 3 min soaking time point onwards (Figures S4A and S4B). The t = 5 min structures were taken to be the fully occupied structures and were refined to 1.62 Å and 1.50 Å for the GES-5-meropenem and GES-5-NA-1-157 complexes, respectively. The electron density for the acylated carbapenems indicated that the intermediates are in the Δ^2 tautomeric conformation, with the C2 atom sp^2 hybridized and the sulfur atom coplanar with the pyrroline ring (Figure S4C). The final $2F_o$-F_c density in the active sites of both complexes is shown in Figures 5A and 5B. The occupancies of the two carbapenems at the t = 5 min time point were also refined. The final values were 0.85 for meropenem and 0.94 for NA-1-157, indicating that

GES-5 was essentially fully acylated by both compounds by this timepoint. The slightly lower occupancy for meropenem may be indicative of some degree of deacylation beginning to take place. The high occupancy of NA-1-157 seems to contradict the kinetic results, which showed that about half of the enzyme was rapidly acylated, with the remaining enzyme acylated slowly over several hours. It is not surprising however, that results from bulk solution differ from those *in crystallo*, resulting primarily from conformational flexibility in the former case. It is possible that in solution the enzyme may be in two or even more different conformational states, one of which may be capable of rapid acylation, while the slow acylation observed could be due to the remaining molecules that are in some alternate conformational state. In *crystallo* however, given the limitations of crystal packing within the lattice, there are two possible scenarios. Crystal growth may be selecting for one enzyme conformation over the other, and in this case the conformation that crystallized is the one capable of rapid acylation. It is also plausible that the initial crystal nuclei forms from enzymes in the rapid acylation conformational state, and this subsequently induces conversion of molecules from the slow to the rapid state as they add to the growing crystal lattice.

In addition to the covalent bond to the side chain of Ser70, the meropenem and NA-1-157 molecules are anchored by hydrogen-bonding interactions in the oxyanion hole between the O7 carbonyl oxygen and the main chain amide nitrogen atoms of Ser70 and Thr237 (Figures 5C and 5D). The C3 carboxylate group on the pyrroline ring interacts with the side chains of Thr235, Thr237, and Arg244. In both complexes a tryptophan residue (Trp105) at the N-terminus of helix α3 (Figure S3) forms one side of the active site, interacting via hydrophobic contacts with the pyrrolidine ring. This residue has been implicated in substrate recognition in various class A β-lactamases, including KPC-2, TEM-1, SME-1, CTX-M, and SHV-2[42-49], through aromatic interactions with the substrates and by changes in the orientation of the indole ring. Analysis of the class A β-lactamase structures available in the PDB (76 unique structures, including six GES enzymes) shows that ~22% have a tryptophan at position 105, while most of the

remaining have a tyrosine. In enzymes with a tryptophan, in the absence of any substrate or inhibitor, the *t-105* rotamer, the third most preferred rotamer after *m95* and *t90*[50], predominates due to the presence of a stabilizing hydrogen bond between the Nε1 atom and the carbonyl oxygen of residue 129 (Ambler residue numbering). Interestingly, in the GES-5-meropenem complex the Trp105 side chain is observed as the *t-105* rotamer, the same as in apo-GES-5[51], whereas in the GES-5-NA-1-157 complex, the residue adopts the *m95* rotamer (Figure 5E). This 120° flip of the Trp105 side chain observed in the GES-5-NA-1-157 complex is likely caused by its C5α-methyl substituent, which could create some steric pressure if Trp105 was in the *t-105* rotamer conformation (Figure 5E). The rotamer flip results in a rotation of the pyrrolidine tail of NA-1-157 relative to that of meropenem by approximately 60° to maintain a face-to-face van der Waals interaction with the indole ring of Trp105.

Superposition of the two complexes (Figure 5E) reveals that there is no appreciable difference in the position and orientation of core of NA-1-157 relative to meropenem (Figure 1A) (*rmsd* = 0.37 Å for 14 common core atoms). To ascertain why meropenem is a substrate for GES-5 while NA-1-157 is a potent inhibitor, we turned to MD simulations of the two carbapenem acyl-enzyme complexes. In both cases the *rmsd*s of the protein main chain relative to the initial model were 1.62 Å and 1.54 Å for meropenem and NA-1-157, respectively, indicating that the simulations were stable for the entire 100 ns (Figure S5), and that there were no major conformational changes. Analysis of the MD trajectory for the GES-5-meropenem complex showed that the 6α-HE group, initially outward-facing relative to the catalytic serine, rotates in towards Lys73 and Glu166 within the first 4 ns (Figures 6A and 6B) and forms a hydrogen bonding interaction with the Oε2 atom of Glu166 (Figures 6C, 6D, and 6E). The hydrogen bond between O62 and the Nδ2 atom of Asn132 is retained when the 6α-HE group rotates (Figure 6E). The C7-C6-C61-C62 torsion angle (Figure 1B), initially at 64°, moves to approximately 163° and remains in this conformation for the duration of the simulation (Figures 6A and 6B). Umbrella sampling of this torsion

angle in the GES-5-meropenem complex shows that the free energy profile (Figure S6) of the rotation is consistent with our observations of the unbiased MD simulation, with a very low free energy barrier (+0.9 kcal mol^{-1}) to traverse from 64° to 163°. Conversely, the 6α-HE group of NA-1-157, also in the outward-facing orientation, does not rotate at any point during the MD simulation, with the C7-C6-C61-C62 torsion, initially at 60°, remaining at an average of 62° (Figures 6A and 6B). With the 6α-HE group in this conformation, the hydrogen bond between O62 of NA-1-157 and the Nδ2 atom of Asn132 is retained throughout the simulation, but there is no contact between O62 and the side chain of Glu166. Umbrella sampling simulations of the C7-C6-C61-C62 torsion angle in the GES-5-NA-1-157 complex shows an energy minimum at ~60° (Figure S6), consistent with the observed crystal structure. In order for the 6α-HE group to rotate to ~160° it must cross a high (+7.5 kcal mol^{-1}) energy barrier at 120°, which would be highly unfavored.

Visual inspection of the MD trajectory for the GES-5-meropenem complex shows that upon rotation of the 6α-HE, a pocket between Glu166, Ser70, and the acyl-enzyme intermediate opens, and a water molecule (designated Wat1) from the TIP3P solvent model enters and remains hydrogen bonded to the glutamate for the duration of the simulation (Figure 7 and Figures S7A and S7B). Moreover, the water molecule is within 4 Å of the C7 atom of the acylated meropenem for the entire time, and is poised perfectly to attack the acyl bond once activated by deprotonation by Glu166 (Figures S7A and S7B). We deem Wat1 to represent the deacylating water molecule. A radial distribution function of the TIP3P solvent relative to the C7 atom of meropenem and the Oε2 atom of Glu166 (Figures S7C and S7D) confirms the presence of the deacylating water in the GES-5-meropenem complex. Conversely, in the GES-5-NA-1-157 acyl-enzyme complex where the 6α-HE does not rotate, formation of the deacylating water pocket is prevented (Figure 7). Inspection of the MD trajectory and calculation of the radial distribution function shows that no external water molecules are observed in the vicinity of the Glu166 side chain.

Although the lack of rotation of the 6α-HE group in the GES-5-NA-1-157 acyl-enzyme complex is clearly preventing deacylation, consistent with the kinetic results, the question remains as to what is interfering with this rotation? In order for the 6α-HE group of either carbapenem to transition from the outward-facing to the inward-facing conformation, the C6-C61 bond can rotate either clockwise or counterclockwise (Figure 8A). When viewed along the bond from C61-C6, a clockwise (negative) rotation in both complexes would be prevented by a severe steric clash between the C62 atom and the Oε2 atom of Glu166, where the distance between them is just above the carbon-oxygen non-bonded contact distance of around 3.2 Å[52] (Figure 8A and 8B). In the GES-5-meropenem and GES-5-NA-1-157 simulations, the high energy barrier (+~8-10 kcal mol^{-1}) (Figure S6) at approximately 0° (equivalent to the C62 atom pointing directly at the Oε2 atom of Glu166) is clearly prohibitive to the rotation of the 6α-HE group in this direction. In the GES-5-NA-1-157 complex, a counter-clockwise (positive) rotation would also be prevented by an internal steric clash between the O62 atom and C51 methyl group, equivalent to the +7.5 kcal mol^{-1} energy barrier seen in umbrella sampling (Figure S6). However, in the GES-5-meropenem complex, there is nothing to prevent the counter-clockwise rotation, and it occurs readily within the first 4 ns of the MD simulation (Figures 6A and 6B).

CONCLUSIONS

In summary, the C5α-methyl substituted carbapenem NA-1-157 possesses potent antimicrobial activity against *E. coli*, *K. pneumoniae*, and *A. baumannii* producing the GES-5 carbapenemase. A competition experiment between NA-1-157 and nitrocefin showed that the compound inactivates the enzyme with high efficiency on a fast time scale ($k_{NA\text{-}1\text{-}157}$ = 4.1 ± 0.8 s^{-1}). Single-turnover kinetics demonstrated that acylation of GES-5 by NA-1-157 resulting in formation of the acyl-enzyme intermediate is biphasic, with a fast phase complete within seconds for roughly half of the enzyme present

in the reaction, while for the remaining, acylation proceeds over the duration of several hours. A jump dilution experiment confirmed that after a short preincubation time (20 s), only half of the inactivated enzyme regained activity. These data suggest that during inactivation, in addition to an irreversible acyl-enzyme intermediate formed during the fast phase of the reaction, another reversible inhibitory complex is also formed. ESI-LC/MS revealed that the latter is also a covalent complex, which could be a reversible tetrahedral intermediate.[39] The GES-5-NA-1-157 acyl-enzyme complex is extremely stable, and for all practical purposes is irreversible, as the deacylation rate constant is only $(2.4 \pm 0.3) \times 10^{-7}$ s^{-1}, which translates to a residence time of 48 ± 6 days. Structural studies and MD simulations demonstrated that the C5α-methyl substituent of NA-1-157 prevents access of a deacylating water to the active site. Introduction of the C5α-methyl group in NA-1-157 gives rise to the unprecedented reversible behavior during acylation of GES-5 and also arrests deacylation of the acyl enzyme.

METHODS

Cloning. For MIC measurements, the wild type gene encoding the mature GES-5 carbapenemase was custom synthesized (Synbio Technologies) with the OmpA leader sequence (a silent mutation was made within the gene to remove an *NdeI* restriction site), and cloned between the *NdeI* and *HindIII* sites of either the pHF016 vector[28] or the pNT221 shuttle vector[27], resulting in plasmids pMT341 and pMT329, respectively. Plasmid pMT341 was introduced into *E. coli* JM83 and *K. pneumoniae* ATCC 13883 by transformation and electroporation, respectively, while plasmid pMT329 was introduced into *A. baumannii* CIP 70.10 by electroporation. Cells were grown in LB containing kanamycin (60 μg/mL for *E. coli* JM83, 10 μg/mL for *K. pneumoniae* ATCC 13883, and 30 μg/mL for *A. baumannii* CIP 70.10) to maintain plasmids. For protein expression, the *E. coli* optimized *ges5* gene[28] was amplified by PCR to remove the first 54 nucleotides encoding the leader sequence and to introduce an *NdeI* restriction site. Subsequently, the fragment was cloned between the *NdeI* and *HindIII* restriction sites in the pET24a(+) expression vector (Novagen), and the sequence was verified by DNA sequencing (McLab). The resulting pNS59 plasmid was transformed into *E. coli* BL21 (DE3).

Antibiotic Susceptibility Testing. MICs were measured in Mueller-Hinton II broth in at least triplicate using the microdilution method according to the CLSI guidelines.[53] Briefly, carbapenems were serially diluted 2-fold in microtiter plates, which were then inoculated with 5×10^5 CFU/mL bacteria. To evaluate whether the interaction between meropenem and NA-1-157 is synergistic, additive, indifferent, or antagonistic, a checkerboard assay was performed.[26] Plates were incubated at 37 °C for 20 h for *E. coli* JM83 and *K. pneumoniae* ATCC 13883 or 24 h for *A. baumannii* CIP 70.10 prior to interpretation. The heat maps were generated by quantitating the cell density in the plates from the checkerboard assay. After subtracting the background, the values were normalized relative to the control well (with no carbapenem)

and averaged (for triplicate measurements) to determine the percent growth. The fractional inhibitory concentration (FIC) index was calculated according to the relationship: FIC index = $FIC_A + FIC_B$, where $FIC_A = MIC_{A+B}/MIC_A$ and $FIC_B = MIC_{B+A}/MIC_B$. The MIC_{A+B} value is the MIC of A in the presence of B, while the MIC_{B+A} value is the MIC of B in the presence of A. FIC index values <0.5 were classified as synergistic.[54]

Protein Expression and Purification. Cells were grown in LB containing 60 µg/mL kanamycin at 37 °C, 190 RPM until an OD_{600nm} of 0.8. Protein overexpression was induced by addition of IPTG (1 mM), the temperature was lowered to at 22 °C, and the cells were grown for an additional 17 h. The cells were harvested by centrifugation at 4000 xg for 10 min and resuspended in 20 mM Tris, pH 7.5. Next, the cell suspension was lysed by sonication, and the soluble fraction was recovered by ultracentrifugation at 32,000 rpm for 1 h at 4 °C. Subsequently, the GES-5 enzyme was purified using ion exchange chromatography as previously described.[29]

Enzyme Kinetics. All reactions were carried out in 50 mM sodium phosphate, 100 mM NaCl, pH 7.0 at 22 °C in triplicate, and data were collected using either a Cary60 (Agilent) or stopped-flow (Bio-Logic) spectrophotometer. Nonlinear regression analyses were performed using Prism 9 (GraphPad Software, Inc.).

Inhibition of GES-5 by NA-1-157. Reactions containing 5-100 µM NA-1-157 were initiated by addition of GES-5 (0.5-10 µM), and the change in absorbance was monitored at 298 nm ($\Delta\varepsilon$ = -10,240 $M^{-1}cm^{-1}$)[24]. Control reactions were run in the absence of GES-5, and the slope of the line was subtracted from the reaction in the presence of GES-5 to correct for nonspecific hydrolysis of NA-1-157.

Determination of the inactivation parameters, $k_{NA\text{-}1\text{-}157}$ and K_I. Competition reactions were carried out using nitrocefin (150 μM) as a reporter (λ = 500 nm, Δε = +15,000 $M^{-1}cm^{-1}$) and contained varying concentrations (0.25-10 μM) of NA-1-157, 1.5 nM GES-5, and 0.2 mg/ml BSA. Progress curves were fitted with Equation 1:

$$A_t = A_0 + v_s t + \frac{v_i - v_s}{k_{inter}} (1 - e^{-k_{inter} t}) \quad (1)$$

where A_t is the absorbance at time t, A_0 is the initial absorbance, v_i is the initial velocity, v_s is the steady-state velocity, and k_{inter} is the first-order rate constant describing the conversion from v_i to v_s. The k_{inter} values were plotted against concentration of NA-1-157 and fitted with Equation 2:

$$k_{inter} = \frac{k_{NA\text{-}1\text{-}157} [I]}{K_I \left(1 + \frac{[S]}{K_m}\right) + [I]} \quad (2)$$

where $k_{NA\text{-}1\text{-}157}$ is the maximum rate of inactivation of both the reversibly and irreversibly inhibited species, K_I is the concentration of NA-1-157 required to reach half of $k_{NA\text{-}1\text{-}157}$, I is the concentration of NA-1-157, S is the concentration of nitrocefin, and K_m for the Michaelis constant of nitrocefin.

Determination of the rate constant for acylation, k_2. Single turnover conditions were utilized to measure k_2. Reactions containing 10 μM NA-1-157 were initiated by addition of GES-5 (50-150 μM), and the change in absorbance was monitored at 298 nm. The time courses for the fast and slow phases of acylation were fitted separately with Equation 3:

$$A_t = (A_0 - A_\infty) e^{-k_{obs} t} + A_\infty \quad (3)$$

where A_t, A_0, and t are as defined above, A_∞ is the final absorbance, and k_{obs} is the apparent rate constant describing acylation. For the fast phase of acylation, the k_{obs} values were plotted versus concentration of GES-5 and fitted with Equation 4:

(4) $$k_{\text{obs}} = \frac{k_2 E}{K' + E}$$

where k_2 is the acylation rate constant for the fast phase of the reaction, E is the concentration of GES-5, and K' is the concentration of GES-5 required to reach ½ of k_{obs}.

Evaluation of the rate constant for deacylation, k_3. The jump dilution method[55] was used to measure recovery of GES-5 activity after incubation with NA-1-157. For the continuous assay, reactions containing 10-15 μM NA-1-157, 2.5-5 μM GES-5, and 0.2 mg/mL BSA were incubated for up to 17 h prior to diluting 10,000-fold into 500 μM nitrocefin containing 0.2 mg/mL BSA, and the absorbance was monitored at 500 nm for up to 2 h. For the discontinuous assay, reactions containing 40 μM NA-1-157, 10 μM GES-5, and 0.2 mg/ml BSA were incubated for 17 h. Subsequently, the mixtures were passed through a Zeba-0.5 mL 7 kDa MWCO spin desalting column (Thermo Fisher) according to the manufacturer's instructions to remove excess inhibitor and then additionally diluted 10,000-fold into buffer containing 0.2 mg/ml BSA. At predetermined time points, the activity was checked by addition of 500 μM nitrocefin containing 0.2 mg/ml BSA. Incubation times and dilutions were varied to ensure maximum inhibition and recovery of activity. Controls were also performed under the same conditions in the absence of the inhibitor. The percentage of activity (determined by comparison to the control reaction) was plotted versus time, and the data were fitted with Equation 5:

(5) $$Y_t = Y_\infty (1 - e^{(-k_3 t)})$$

where Y_t is the percentage of activity at time t, Y_∞ is the final percentage of activity, and k_3 is the deacylation rate constant.

ESI-LC/MS. GES-5 (2 μM) was incubated with NA-1-157 (10 μM**)** in 50 mM NaPi, 150 mM NaCl, pH 7 at 25 °C. Aliquots were removed at 20 s and 1 h, quenched with 10% acetonitrile/0.1% formic acid, and

stored at -80 °C until analysis. For the reactions where NA-1-208 was added, the reaction was performed as described above. Aliquots were removed at 30 s, 2 min, and 2 h and immediately passed through two successive Zeba-0.5 mL 7 kDa MWCO spin desalting columns to remove unbound NA-1-157. Next, an excess of NA-1-208 (10-fold above its K_i value) was added, and the reaction was incubated for an additional 30 min at 22 °C. Subsequently, the reaction was quenched with 10% acetonitrile/0.1% formic acid and stored at -80 °C until analysis. All reactions were performed in triplicate. A control reaction performed in the absence of NA-1-157 showed that all enzyme was present in a covalent complex with NA-1-208. For ESI-LC/MS analysis, a Dionex UltiMate 3000 LC system was coupled with a Bruker micrOTOF-QII mass spectrometer that was run in the positive-ion mode as follows: end plate offset voltage = -500 V, capillary voltage = 2000 V, and nitrogen as both a nebulizer (4 bar) and dry gas (8 L/min) at 180 °C. The Hystar 5.0 SR1 software was used, and mass spectra were collected over the mass range of 400-3000 m/z. For LC separations, an Agilent Poroshell 300SB-C3 (5 µm, 2.1 mm i.d. x 75 mm) column was used at 40 °C with the following program: 2 min hold at 90%A/10%B, followed by a linear gradient from10-90%B from 2-13 min, followed another 2 min hold at 90%A/10%B (A = 0.1% formic acid in water, B = 0.1% formic acid in acetonitrile) with a flow rate of 0.4 mL/min. For the first 2 min of the run, LC flow was diverted to the waste. The maximum entropy algorithm (Compass DataAnalysis) was used to deconvolute multiply charged ions. Percentages of the GES-5-NA-1-157 and GES-5-NA-1-208 complexes were calculated by dividing the relative peak height(s) of each species by the total sum of all peak heights for both species. For the GES-5-NA-1-157 complex, peak heights of all three observed species (29,471 Da, 29,487 Da, and 29,629 Da) were used for the calculation.

X-ray Crystallography. The GES-5 protein was dialyzed against 20 mM HEPES, pH 7.6 and concentrated to 15 mg/ml. Crystals appeared spontaneously in this buffer, and were transferred to a

stabilization solution comprising unbuffered 0.2 M ammonium iodide and 20% PEG 3350 augmented with 30% ethylene glycol. These crystals belonged to space group $P2_12_12_1$ with cell dimensions approximately 76.8 x 80.6 x 87.3 Å, containing two independent GES-5 molecules in the asymmetric unit. The crystals were isomorphous with those reported for several GES enzymes, including apo-GES-5[51] (PDB code 4GNU). The GES-5-meropenem and GES-5-NA-1-157 complexes were prepared by soaking the pre-formed apo-GES-5 crystals in stabilization solution containing 10 mM of either meropenem or NA-1-157. The crystals were soaked for 1 min, 2 min, 3 min, 5 min, and 10 min, and then flash-cooled in liquid nitrogen and stored for X-ray diffraction studies.

Data sets for the GES-5-NA-1-157 complexes at the various timepoints were collected on SSRL beamline BL12-2 using X-rays at 12658 eV (0.9746 Å) and a Pilatus 6M PAD detector running in shutterless mode. A total of 1800 images were collected for each of the crystals used, and the data were processed and scaled using XDS[56] and AIMLESS[57]. Data sets for the GES-5-meropenem complexes at various time points were collected on ALS beamline 5.0.3 using X-rays at 12700 eV (0.97625 Å) using a Pilatus3 2M PAD detector. A total of 1080 images were collected for each crystal, and the data were processed and scaled using *autoPROC*[58]. All structures were solved by molecular replacement (MR) using the apo-GES-5 structure (PDB code 4GNU) as the starting model with all water molecules and ions removed. The structures were refined with *phenix.refine*[59] with the covalent bond between the C7 atom of meropenem and NA-1-157, and the Oγ atom of Ser70, restrained at 1.42 Å. Model building was completed with COOT[60]. Data collection and refinement statistics are given in Table 4.

Computational methods. Figures were generated with PYMOL (Schrodinger). Docking of intact (non-hydrolyzed) meropenem and NA-1-157 to apo-GES-5 was carried out with ICM-Pro 3.8-6a (Molsoft)[61-62]. Apo-GES-5 (PDB code 4GNU) was converted to an ICM object, with optimization of hydrogen atom

placement. The GES-5-imipenem structure (PDB Code 4H8R) was superimposed and used to define an initial position for the substrate binding site in the apo-GES-5 receptor. The docking runs were performed multiple times into both molecules in the apo-GES-5 asymmetric unit, and the most energetically-favored binding modes were extracted from ICM-Pro as PDB files.

MD simulations were performed in triplicate for 100 ns on the GES-5-meropenem and GES-5-NA-1-157 Michaelis complexes derived from docking, and the meropenem and NA-1-157 acyl-enzyme 5 min crystal structures. The models were prepared with Maestro (Schrodinger) using the OPLS3e force field[63], and the pre-defined TIP3P water model[64] was used to build the system. The overall charges of the models were neutralized with Na+ and Cl^- ions, and 0.15 M NaCl was added prior to building the system. The systems were minimized prior to the final 100 ns production step run at 300 K and 1 Atm pressure, using the Nosé–Hoover chain coupling scheme for temperature control and the Martyna–Tuckerman–Klein chain coupling scheme with a coupling constant of 2.0 ps for pressure control[65]. Nonbonded forces were calculated using an r-RESPA integrator. The MD simulations were performed using Desmond[66] in the Schrodinger 2019-2 release, and the trajectories were saved at 10 ps intervals for analysis. Analyses were carried out in Maestro using the Simulation Interactions Diagram, Simulation Event Analysis and Radial Distribution Function widgets. Maestro and Desmond were run on the SHERLOCK 3.0 HPC cluster at Stanford University.

6α-HE Umbrella Sampling Simulations. Crystal structures of GES-5-NA-1-157 (PDB 8V9H) and GES-5-meropenem (PDB 8V9G) were chosen as initial structures for the simulations. All crystallographically observed water molecules solvating chain A of each structure were retained. The PropKa 3.1 server[67] was used to determine the protonation states of all titratable residues. The all-atom AMBER ff14SB force field described standard protein residues[68]. The acylated NA-1-157 and meropenem non-standard residues were parameterized using General Amber Force Field (GAFF) in the antechamber program in AmberTools20[69].

Partial charges were generated for both ligands using restrained electrostatic potential fitting (RESP) implemented in the R.E.D. server[70]. Each system was solvated in a 10 Å water box of TIP3P[64] water molecules using the tleap program in the AmberTools20 package[71]. The charge of the system was neutralized using Na^+ and Cl^- to a concentration of approximately 180 mM. Starting structures underwent an energy minimization with 300 steps of steepest descent and 1000 steps of conjugate gradient with restraints on all protein heavy atoms of 100 kcal mol^{-1} $Å^{-2}$. A second minimization step was run with only protein backbone atoms restrained (100 kcal mol^{-1} $Å^{-2}$) with 300 steps of steepest descent and 1000 steps of conjugate gradient. The system was heated to 298 K from 25 K within 20 ps in the NVT ensemble with restraints on Cα atoms of 5 kcal mol^{-1} $Å^{-2}$. The system was then equilibrated over 500 ps in the NPT ensemble at 298 K (Langevin thermostat with a collision frequency of 5 ps^{-1}) and 1 atm of pressure (Berendsen barostat, coupling constant of 2 ps). Restraints on Cα atoms (5 kcal mol^{-1} $Å^{-2}$) were removed after 250 ps. A 100 ns production MD simulation was run in the NPT ensemble to generate starting conformations for the umbrella sampling simulations, using the PMEMD engine of the AMBER 20 package.

Umbrella sampling simulations were run with the rotation of the C7-C6-C61-C62 torsion angle as the reaction coordinate. 1 ns of sampling was performed for each umbrella sampling window (every 10° from -180° to 180°) with a 100 kcal mol^{-1} $Å^{-2}$ force constant on the dihedral angle. No other restraints were employed. The potential of mean force (PMF) around the C7-C6-C61-C62 torsion angle was calculated using the weighted-histogram analysis method (WHAM)[72]. The final energy profile for C7-C6-C61-C62 torsion rotation for both compounds was calculated by averaging the free energy profile of 5 independent repeats from different starting structures (the equilibrated system, after 25 ns of production simulation, after 50 ns of production simulation, after 75 ns of production simulation, and after 100 ns of production simulation).

ANCILLARY INFORMATION

Supporting Information. Heat maps from the checkerboard assay used to determine FICI for meropenem and NA-1-157, MS analysis of the GES-5-NA-1-157 and GES-5-NA-1-208 complexes, ribbon structure of the putative GES-5-NA-1-157 Michaelis complex from MD simulation, initial F_o-F_c electron density maps of GES-5-NA-1-157 and GES-5-meropenem acyl-enzyme complexes, plot of *rmsd* of the GES-5 main chain versus time for the GES-5-NA-1-157 and GES-5-meropenem acyl-enzyme complexes, plots of water molecule distribution analysis in the GES-5-NA-1-157 and GES-5-meropenem acyl-enzyme complexes, plot of free energy change of rotation of 6α-HE group, table showing molecular docking results from ICM-Pro, movie showing MD simulation of the GES-5-meropenem Michaelis complex, movie showing MD simulation of the GES-5-NA-1-157 Michaelis complex.

PDB ID Codes. The GES-5-meropenem and GES-5-NA-1-157 structure factors and atomic coordinates have been deposited in the Protein Data Bank with PDB codes 8V9G and 8V9H, respectively. The authors will release the atomic coordinates and experimental data upon article publication.

Corresponding Author Information. John D. Buynak, buynak@smu.edu, Clyde A. Smith, csmith@slac.stanford.edu, Sergei B. Vakulenko, svakulen@nd.edu.

Acknowledgements. This work was supported by the grant 1R01AI155723 from the National Institutes of Health/National Institute of Allergy and Infectious Diseases (NIH/NIAID) to SBV and JDB and grants 1R01AI174599 and 1R15AI42699 from the NIH/NIAID to JDB. MB is supported by BBSRC Funded

SWBio Doctoral Training Partnership [BB/T008741/10]. Umbrella sampling simulations were carried out using the computational facilities of the Advanced Computing Research Centre, University of Bristol (http://www.bristol.ac.uk/acrc/). Portions of this research were carried out at the Stanford Synchrotron Radiation Lightsource (SSRL), a national user facility operated by Stanford University on behalf of the U.S. Department of Energy. Use of SSRL is supported by the U.S. Department of Energy, Office of Science, Office of Basic Energy Sciences under Contract No. DE-AC02-76SF00515. The SSRL Structural Molecular Biology Program is supported by the DOE Office of Biological and Environmental Research, and by the National Institutes of Health, National Institute of General Medical Sciences (P30GM133894).

Abbreviations Used. PBPs, penicillin-binding proteins; DBOs, diazobicyclooctanes; MR, molecular replacement; CLSI, Clinical and Laboratory Standards Institute; MD, molecular dynamics; ESI-LC/MS, electrospray ionization-liquid chromatography/mass spectrometry, *rmsds*, root mean squared deviations; 6α-HE, 6α-hydroxyethyl.

Notes. The authors declare no competing financial interest.

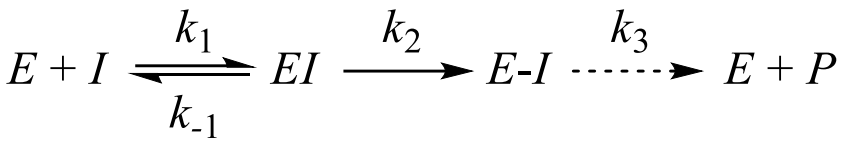

Scheme 1. Minimal enzymatic pathway for inhibition of GES-5 by NA-1-157. E is the enzyme, I is the inhibitor, *EI* represents the complexes formed prior to acylation, *E-I* is the acyl-enzyme complex, and P is the hydrolyzed inhibitor. The dashed arrow signifies that only extremely slow deacylation was observed.

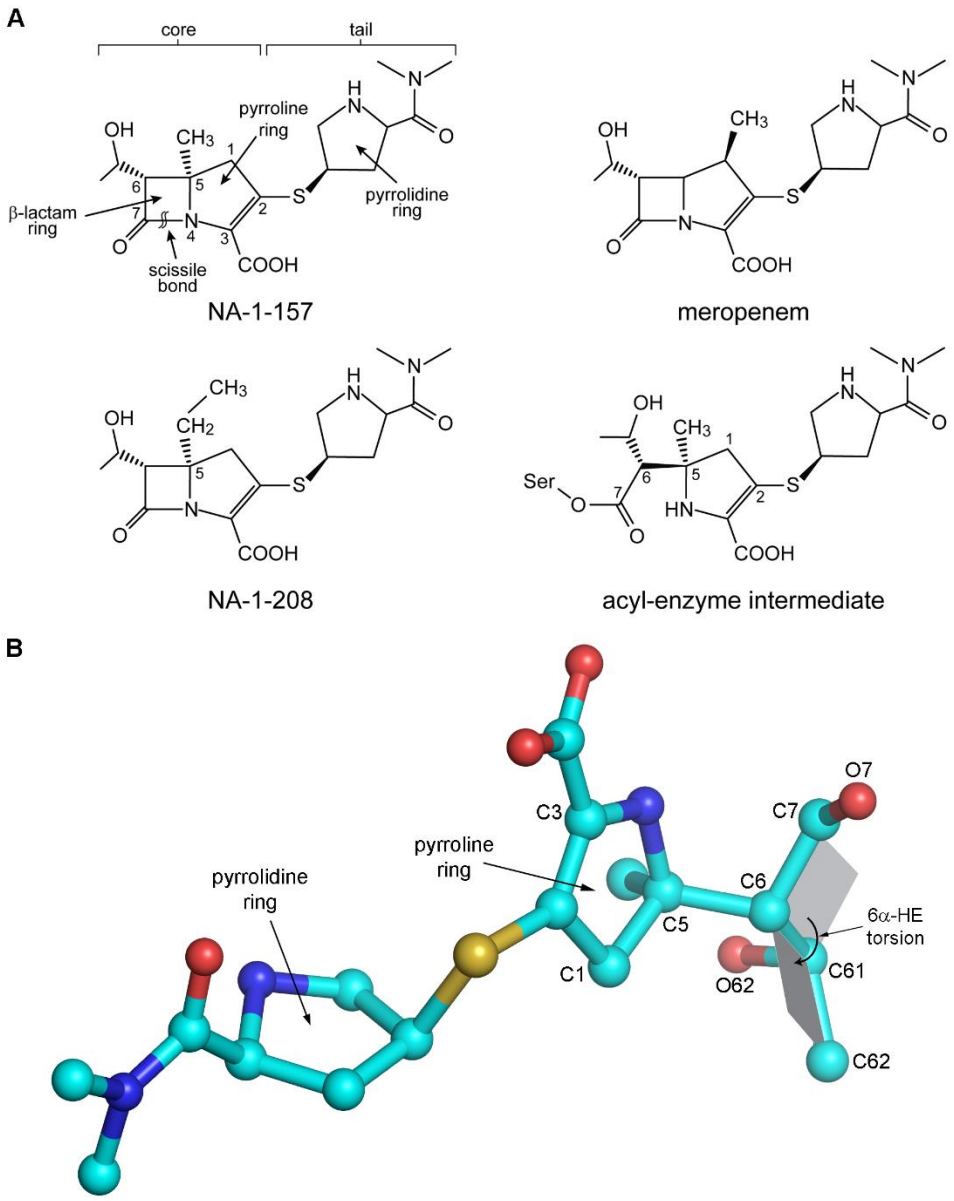

Figure 1. Structures of carbapenems. A) NA-1-157, NA-1-208, meropenem, and the NA-1-157 acyl-enzyme intermediate. The core and tail regions are indicated, and atom numbering of some core atoms is shown. **B)** Structure of hydrolyzed NA-1-157 derived from the GES-5-NA-1-157 crystal structure. Two planes (gray) representing C7-C6-C61 and C6-C61-C62 are indicated. The dihedral angle between these two planes is measured as the C7-C6-C61-C62 torsion angle (labeled as the 6α-HE angle) in COOT and Desmond. The 6α-HE torsion angle as indicated here is approximately 130°.

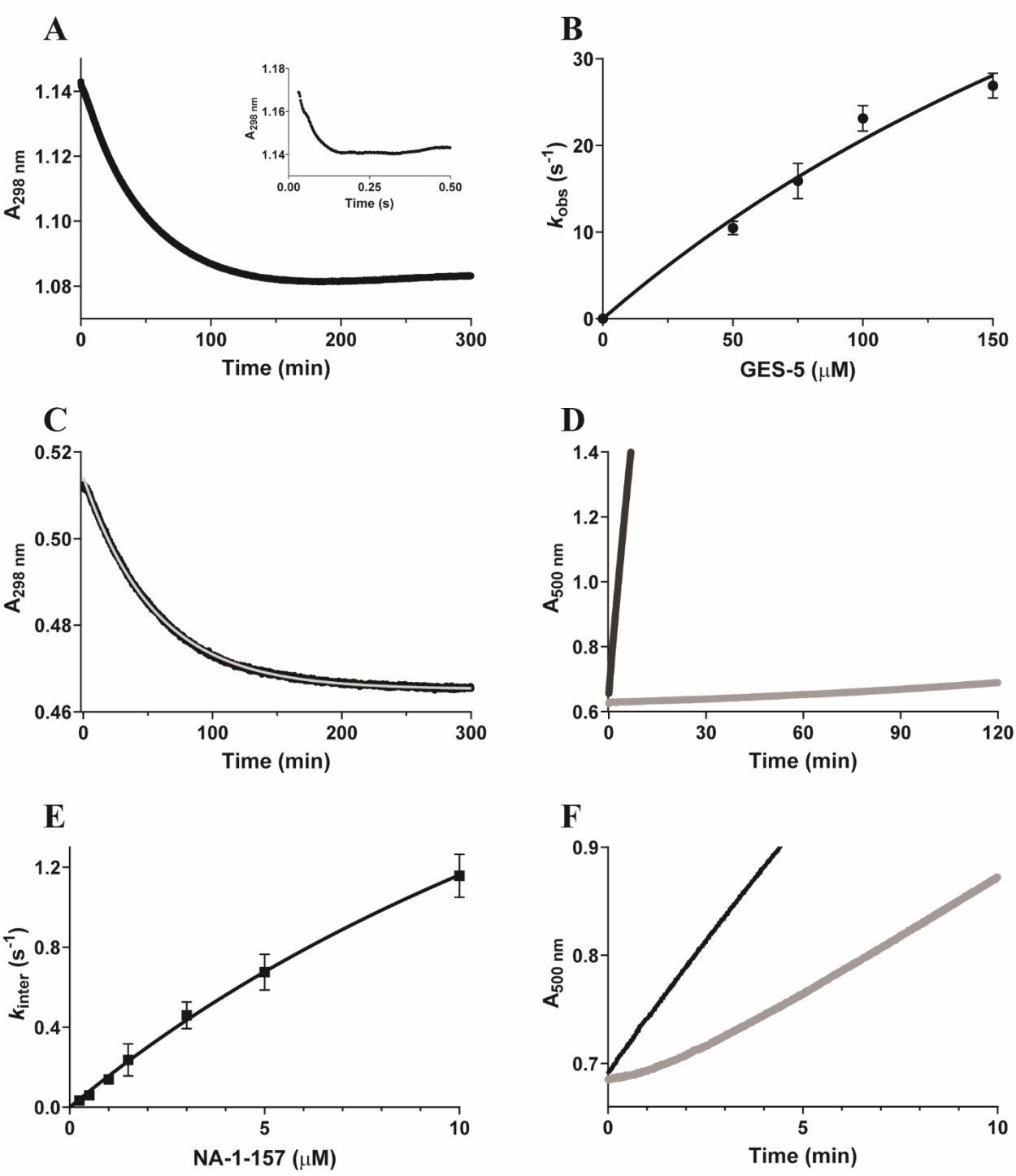

Figure 2. Kinetics of the GES-5-NA-1-157 interaction. A) Representative progress curves of the reaction between GES-5 (10 μM) and NA-1-157 (100 μM). The inset shows the fast phase of the reaction measured using a stopped-flow instrument. **B)** Plot of k_{obs} versus concentration of GES-5 to determine the

$k_{2\ fast}$ acylation rate constant. The line of best fit is shown in black. **C)** Representative progress curve showing the slow phase of acylation of GES-5 by NA-1-157 under single-turnover conditions to evaluate the $k_{2\ slow}$ acylation rate constant. The line of best fit is shown in gray. **D)** Time course for recovery of GES-5 activity after overnight preincubation in the presence (gray line) and absence (black line) of NA-1-157 and subsequent jump dilution. **E)** Plot of k_{inter} versus concentration of NA-1-157 to determine the inactivation parameters $k_{NA\text{-}1\text{-}157}$ and K_I. The line of best fit is shown in black. **F)** Time course for recovery of GES-5 activity after 20 s preincubation in the presence (gray line) and absence (black line) of NA-1-157 and subsequent jump dilution.

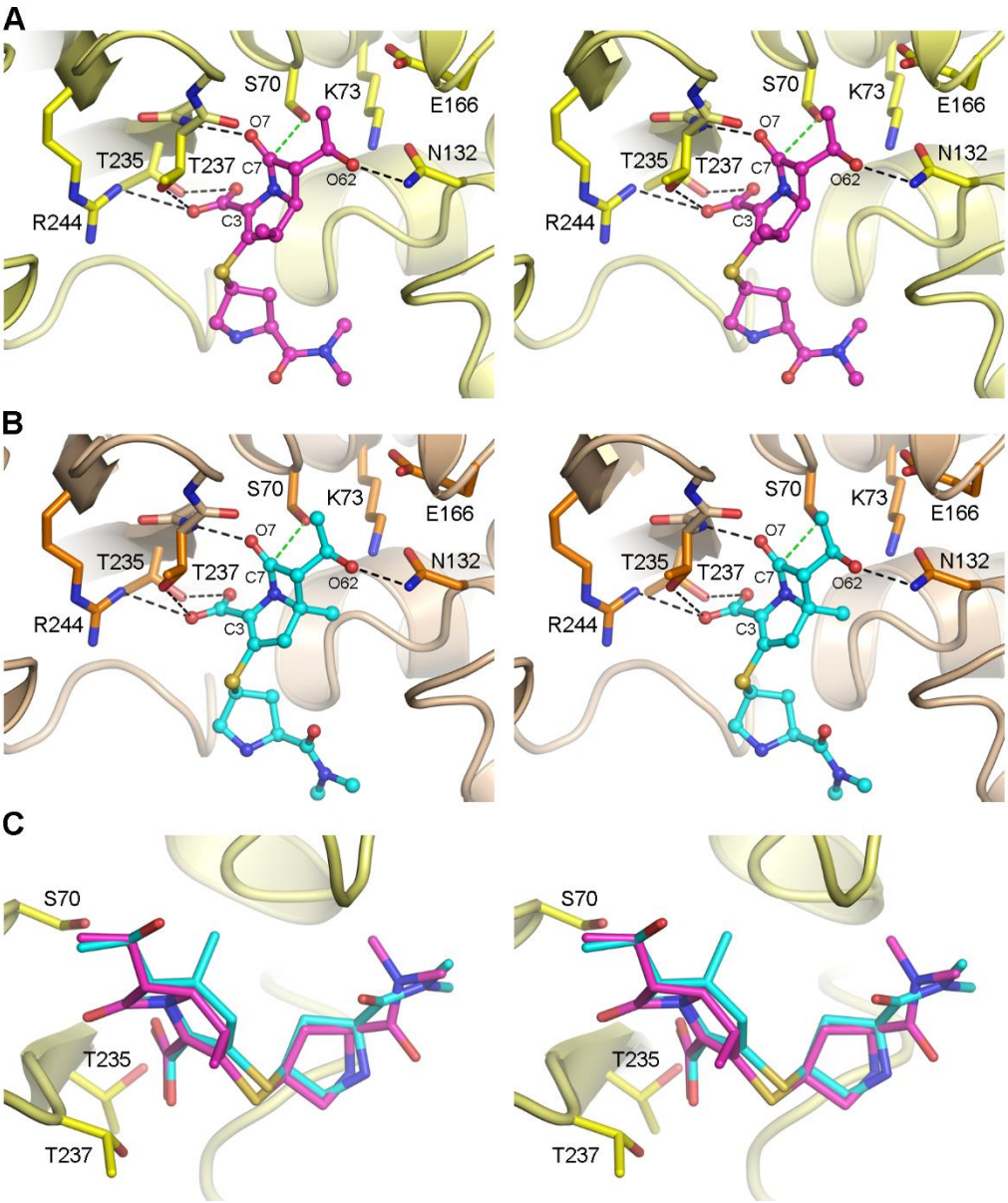

Figure 3. Structure of the GES-5-meropenem and GES-5-NA-1-157 Michaelis complexes. A) Stereoview of docked non-hydrolyzed meropenem (magenta balls and sticks) in the active site of apo-GES-5 (yellow ribbons and sticks). **B)** Stereoview of docked non-hydrolyzed NA-1-157 (cyan balls and sticks) in the active site of apo-GES-5 (brown ribbons and orange sticks). In panels **A** and **B**, hydrogen bonds are shown as dashed black lines, while the green dashed lines indicate the close approach of the β-lactam C7 atom to the Oγ of the catalytic serine (Ser70). **C)** Stereoview of the superposition of meropenem (magenta) and NA-1-157 (cyan) in the active site of apo-GES-5.

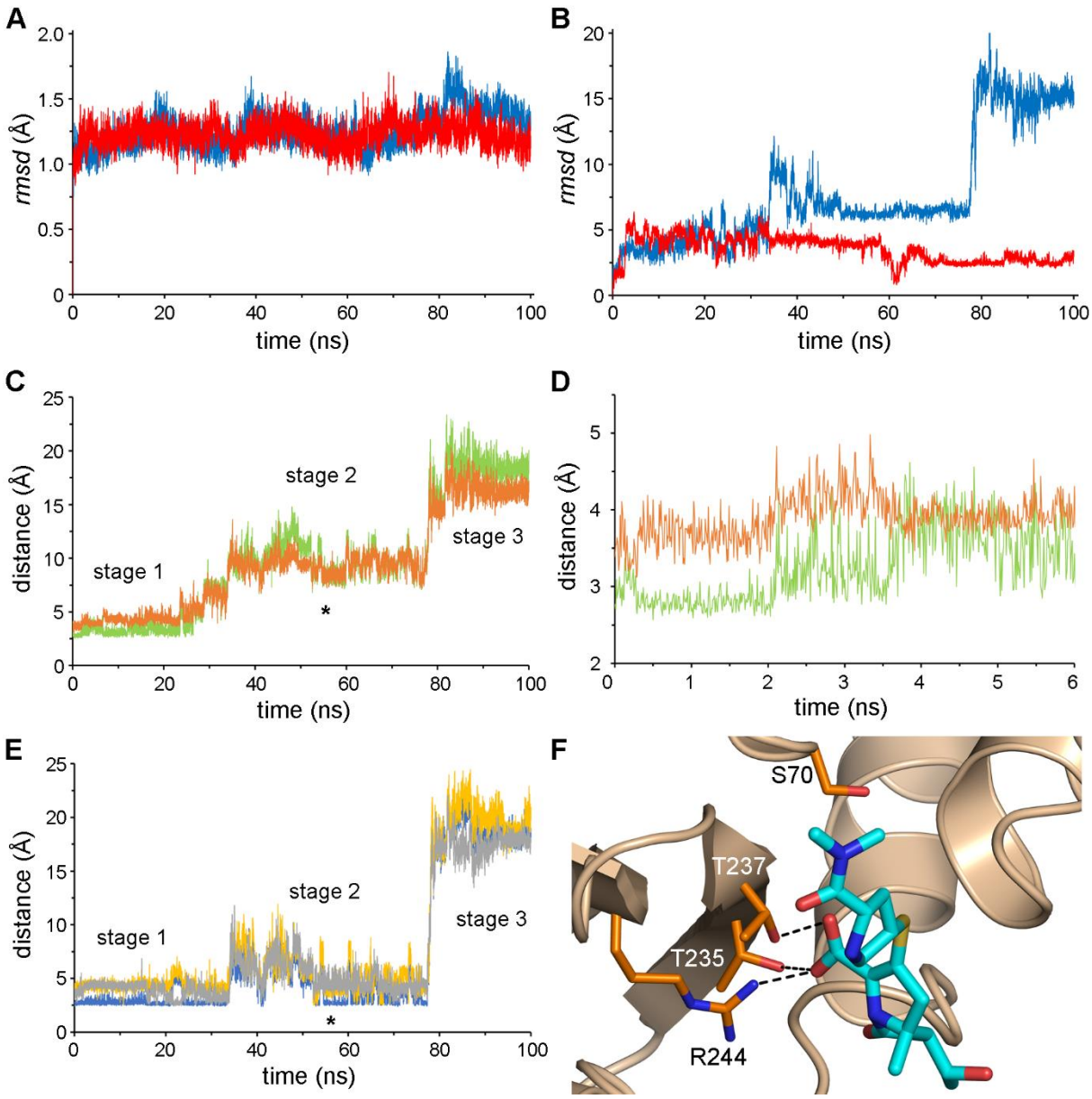

Figure 4. MD simulation of the GES-5-meropenem and GES-5-NA-1-157 Michaelis complexes. A) Plot of the *rms* deviation (*rmsd*) of the main chain for the GES-5 receptor with meropenem (red) and NA-1-157 (blue) over the course of 100 ns MD simulation with Desmond. The *rmsd*s were calculated for each 10 ps time point using the structures at $t = 0$ as the reference. The simulations converge early and remain stable over the full 100 ns. **B)** Plot of the *rmsd* of the meropenem (red) and NA-1-157 (blue) molecules relative to their starting configurations at $t = 0$. While meropenem (red) remains in essentially the same position, NA-1-157 (blue) moves in two distinct stages. **C)** Plot of two distances between NA-1-157 and

GES-5; O7-N(Thr237) (green trace) and C7- Oγ(Ser70) (orange trace), monitoring the position of the β-lactam group during the 100 ns MD simulation. **D)** Expanded view of plot shown in panel **C** to show the first 6 ns. **E)** Plot of three distances between NA-1-157 and GES-5; O31-Nη1(Arg244) (blue trace), O31-Oγ1(Thr237) (yellow trace), and O32-Oγ1(Thr235) (gray trace), monitoring the position of the C3 carboxylate group during the 100 ns MD simulation. **F)** The interaction of NA-1-157 with GES-5 at the 55 ns timepoint (the asterisk in panels **C** and **E**), showing hydrogen bonds (black dashed lines) between the C3 carboxylate of NA-1-157 and residues on the protein.

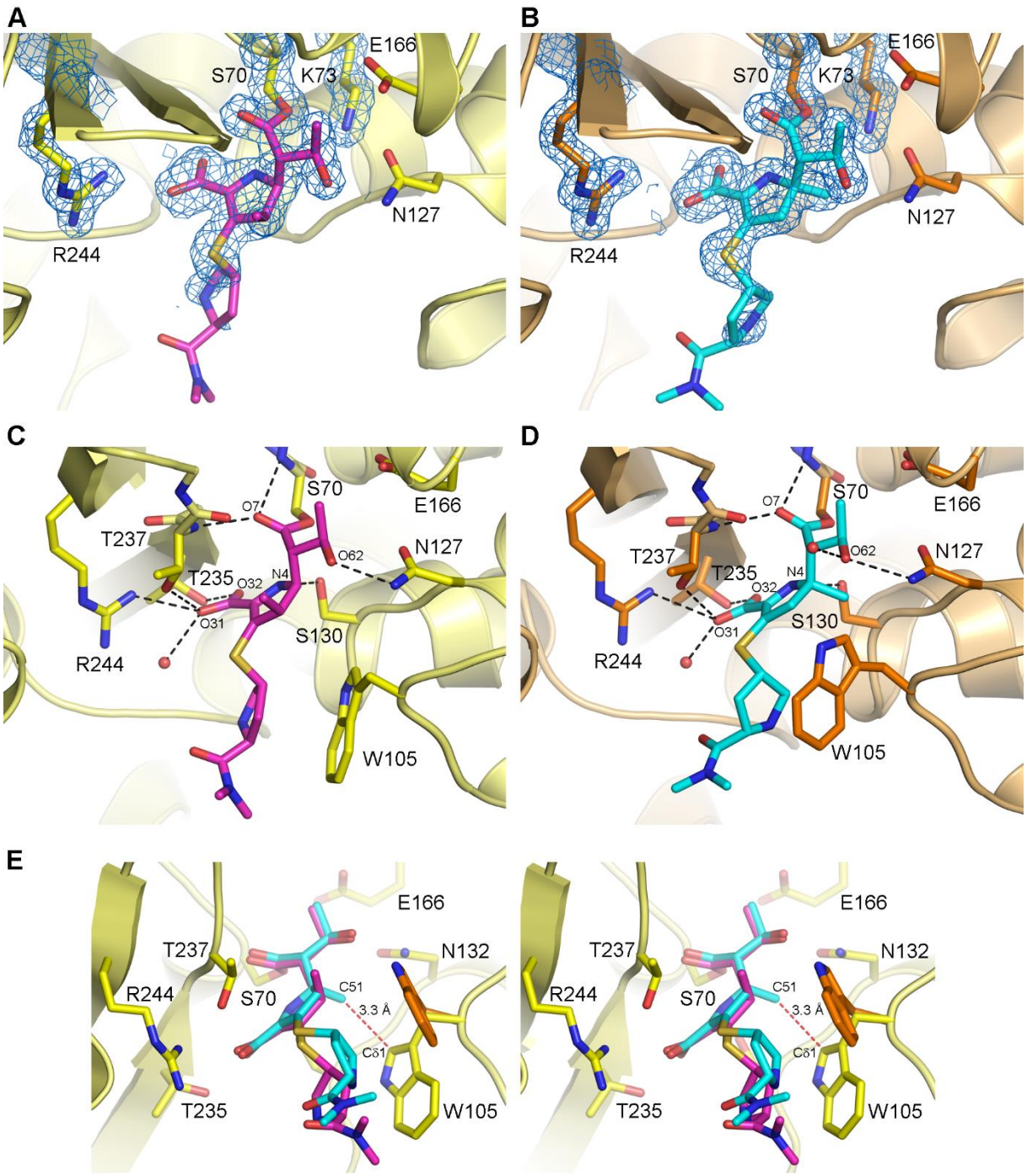

Figure 5. The GES-5-meropenem and GES-5-NA-1-157 acyl-enzyme structures. A) Final $2F_o$-F_c electron density (blue mesh, 1.0 σ) for meropenem (magenta sticks) in the active site of GES-5 (yellow ribbons and sticks). The $2F_o$-F_c density is also shown for three residues, Ser70, Lys73, and Arg244. **B)** Final $2F_o$-F_c electron density (blue mesh, 1.0 σ) for NA-1-157 (cyan sticks) in the active site of GES-5

(brown ribbons and orange sticks). The $2F_o$-F_c density is also shown for three residues, Ser70, Lys73, and Arg244. **C)** Hydrogen bonding interactions (black dashed lines) of meropenem (magenta sticks) in the final GES-5-meropenem structure. **D)** Hydrogen bonding interactions (black dashed lines) of NA-1-157 (cyan sticks) in the final GES-5-NA-1-157 structure. **E)** Stereoview of the GES-5-meropenem active site with the GES-5-NA-1-157 complex superimposed. Meropenem is colored magenta and NA-1-157 is cyan. Only the enzyme in the meropenem complex is shown (yellow ribbons and sticks) for clarity, except for the side chain of Trp105 which is shown as orange sticks for the GES-5-NA-1-157 complex. The potential close approach of the C5α methyl (C51) to the Trp105 side chain in the GES-5-meropenem complex is indicated by a dashed red line. The distance of this clash (3.3 Å) is just shorter than the van der Waals carbon-carbon non-bonded contact distance of 3.4 Å.

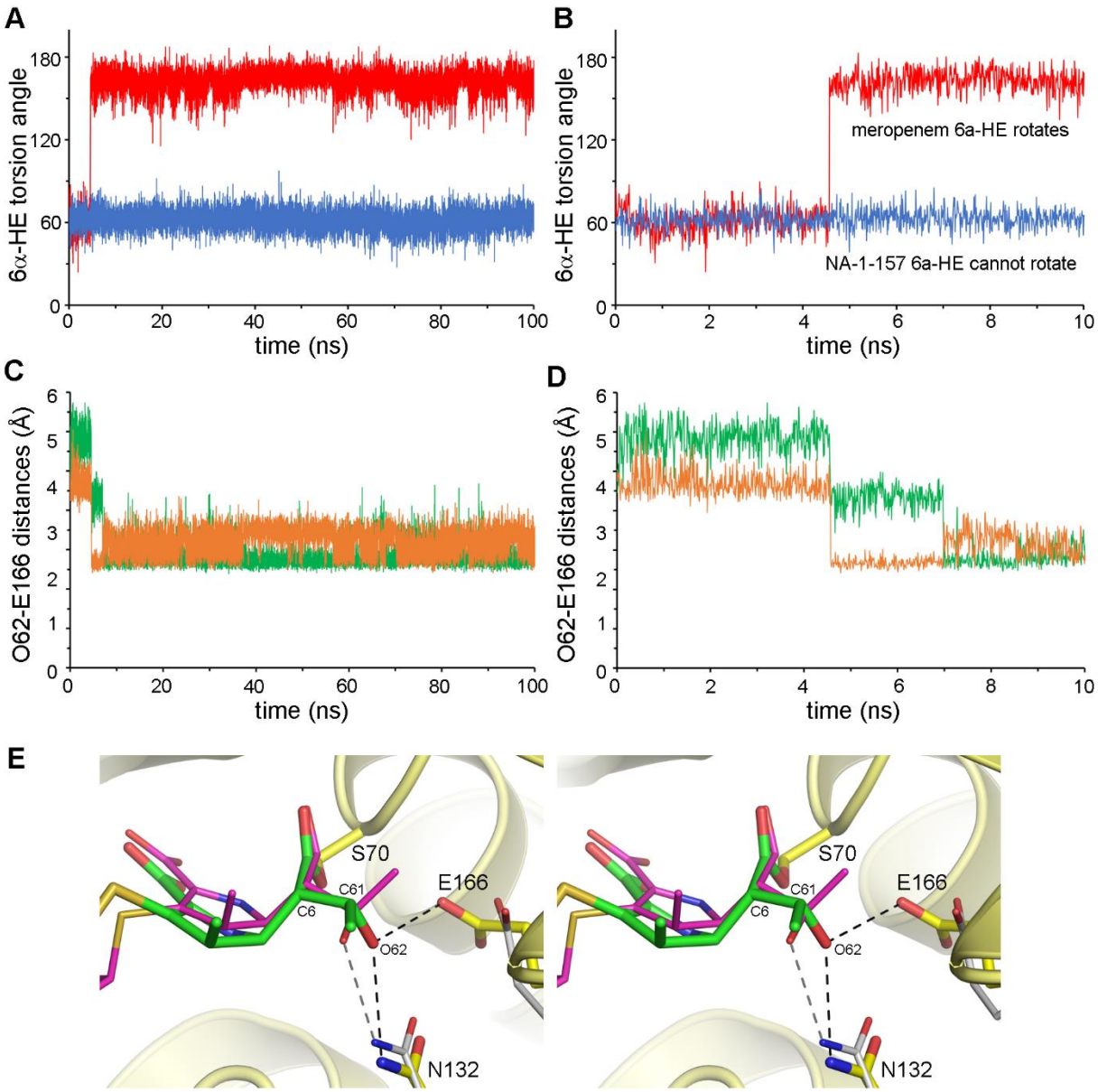

Figure 6. Molecular dynamics of the GES-5-meropenem and GES-5-NA-1-157 acyl-enzyme complexes. A) Plot of the 6α-HE group torsion angles for meropenem (red trace) and NA-1-157 (blue trace) over the 100 ns MD simulations. **B)** Expanded view of plot shown in panel **A** showing the sudden rotation of the 6α-HE group in the GES-5-meropenem complex at approximately 4.5 ns. This rotation moves the 6α-HE group from the outward-facing conformation to the inward-facing conformation. **C)** Plot of the distances between the O62 atom of meropenem and the Oε1 (green trace) and Oε2 (orange

trace) of Glu166 of GES-5 over the 100 ns MD simulations. **D)** Expanded view of plot shown in panel **C** to show the first 10 ns. The formation of a O62-Oε2(Glu166) hydrogen bond is observed at approximately 4.5 ns. Rotation of the carboxylate of Glu166 after 7 ns results in the switch to a O62-Oε1(Glu166) hydrogen bond. **E)** Stereoview of the GES-5 active site (yellow ribbons and sticks at t = 0 and gray thin sticks at t = 4.6 ns) with meropenem (magenta thin sticks at t = 0 and green sticks at t = 4.6 ns) before and after the 6α-HE group torsion angle rotation. The Asn132 side chain is also shown at both timepoints (yellow at t = 0 and gray at t = 4.6 ns). The O62-Nδ2(Asn132) hydrogen bond (initially indicated by a gray dashed line at t = 0) is maintained during the 6α-HE group rotation, and is shown as a black dashed line at t = 4.6 ns.

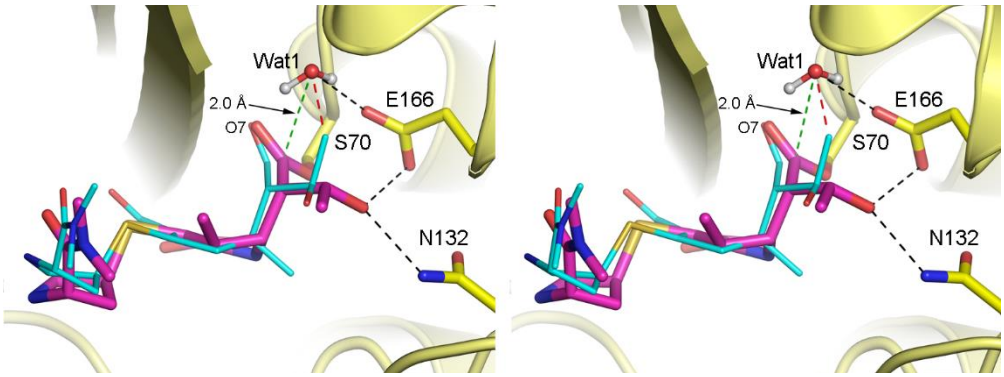

Figure 7. The deacylating water pocket. Stereoview of the superposition of NA-1-157 (thin cyan sticks) onto meropenem (magenta sticks) in the active site of the GES-5-meropenem complex (yellow ribbons and sticks). The PDB files for both complexes were extracted from the respective MD trajectories at the timepoint *t* = 5 ns. In the meropenem-GES-5 complex, the 6α-HE group of meropenem has rotated inwards with the O62-Oε2(Glu166) hydrogen bond present at this timepoint. A water molecule (Wat1) has entered near the glutamate side chain into a position poised to hydrolyze the acyl bond (as indicated by the green dashed line with a distance of 3.6 Å). Conversely, in the GES-5-NA-1-157 complex, the 6α-HE group of NA-1-157 is outward-facing and the C62 atom points up towards the deacylating water pocket, which would prevent the entrance of a water molecule (red dashed line). Hydrogen bonds are shown as black dashed lines.

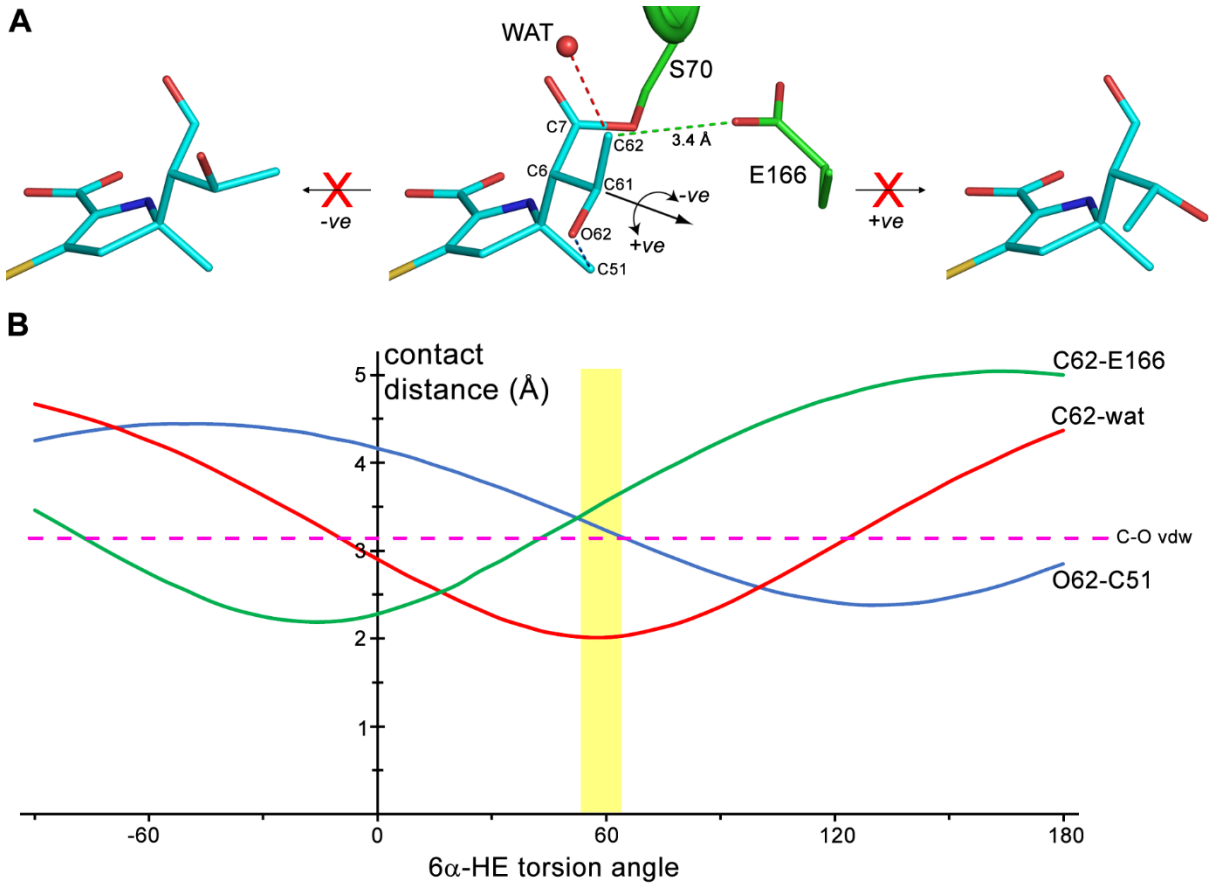

Figure 8. Rotational flexibility of the 6α-HE group of NA-1-157 is restricted. **A)** In the GES-5-NA-1-157 acyl-enzyme complex (center), rotation of the 6α-HE group about the C6-C61 bond is sterically restricted in both the clockwise (-ve) direction by a C62-Glu166 clash (green dashed line and left panel) and in the counter-clockwise (+ve) direction by a O62-C51 clash (blue dashed line and right panel). Only the conformation observed in the crystal structure (center) is allowed. In this conformation, the C62 atom prevents a water molecule from entering the active site to facilitate deacylation. **B)** Plot of the three distances shown as dashed lines in panel **A** as a function of the 6α-HE torsion angle (see Figure 1B). The dashed magenta line represents the carbon-oxygen van der Waals non-bonded contact distance (approx. 3.2 Å). Distances below these lines are sterically disallowed. The yellow rectangle shows that rotation of the 6α-HE group in the GES-5-NA-1-157 complex can occur only in a very limited range due to steric hinderance with either Glu166 or the C5α methyl group of NA-1-157.

Table 1. MICs (μg/mL) of carbapenems alone and in combination.

Strain	Carbapenem	MIC (μg/mL)
E. coli JM83 (GES-5)	MEM[a]	2
	NA-1-157	0.5
	MEM + 0.25 μg/mL NA-1-157	0.031 (64)[b]
	MEM + 0.125 μg/mL NA-1-157	0.125 (16)
	MEM + 0.062 μg/mL NA-1-157	0.5 (4)
E. coli JM83 (control[c])	MEM	0.031
	NA-1-157	0.5
K. pneumoniae ATCC 13883 (GES-5)	MEM	2
	NA-1-157	0.5
	MEM + 0.25 μg/mL NA-1-157	0.031 (64)
	MEM + 0.125 μg/mL NA-1-157	0.062 (32)
	MEM + 0.062 μg/mL NA-1-157	0.5 (4)
K. pneumoniae ATCC 13883 (control[c])	MEM	0.031
	NA-1-157	0.5

[a]MEM, meropenem.

[b]The fold difference relative to the MEM MIC is given in parenthesis.

[c]Parental strain not expressing any β-lactamase.

Table 2. MICs (µg/mL) of carbapenems against *A. baumannii* CIP 70.10 expressing the GES-5 carbapenemase.

	MIC (µg/mL)	
Carbapenem [a]	GES-5	Control[b]
NA-1-157	2	0.5
MEM	32	0.5
IPM	16	0.25

[a]MEM, meropenem; IPM, imipenem.

[b]Parental *A. baumannii* CIP 70.10 strain that does not produce any β-lactamase from the shuttle vector.

Table 3. Pre-steady-state kinetic parameters for the interaction between GES-5 and carbapenems.

	Carbapenem[a]		
Parameter	NA-1-157	MEM[b]	IPM[b]
$k_{2\ fast}$ (s^{-1})	99 ± 31	> 97 ± 2	> 450 ± 10
$k_{2\ slow}$ (s^{-1})	$(2.6 \pm 0.1) \times 10^{-4}$	0.087 ± 0.001	0.35 ± 0.01
k_3 (s^{-1})	$(2.4 \pm 0.3) \times 10^{-7}$	0.10 ± 0.01	0.45
residence time (s)	$(4.2 \pm 0.5) \times 10^{6}$	10 ± 1	2.4

[a]MEM, meropenem; IPM, imipenem.

[b]These data were previously reported.[29]

Table 4. Data collection and refinement statistics for the acyl-enzyme complexes of GES-5 with meropenem (MEM) and NA-1-157[a].

		MEM	NA-1-157
Data Collection			
Space group		$P2_12_12_1$	$P2_12_12_1$
Unit cell, a, b, c (Å)		76.83, 80.58, 87.33	76.73, 80.38, 87.71
Resolution (Å)		59.2–1.62 (1.65–1.62)	38.5–1.50 (1.53–1.50)
Reflections	- observed	691279	834326
	- unique	69480	87364
R_{meas}[b]		0.106 (1.34)	0.094 (1.15)
R_{pim}[c]		0.035 (0.428)	0.031 (0.416)
$I / \sigma I$		14.8 (2.1)	15.2 (1.9)
Completeness (%)		99.9 (99.9)	99.9 (99.7)
CC½[d]		0.999 (0.778)	0.999 (0.803)
Average multiplicity		9.9 (10.3)	9.5 (9.3)
Wilson B (Å^2)		20.0	19.7
Refinement			
PDB Code		8V9G	8V9H
R_{work} / R_{free}[e]		0.1748 / 0.2182	0.1614 / 0.1917
Reflections, work/free		69401 / 3458	87357 / 4670
Number of atoms	- protein	4062	4114
	- water	247	382
	- ligands	52	52
B-factors (Å^2)	- protein	22.4	20.9
	- water	31.0	31.5
	- ligands	34.7	26.0
rms deviations	- bond lengths (Å)	0.006	0.006
	- bond angles (º)	1.12	1.09
Ramachandran plot[f]	- favored (%)	98.3	98.48
	- outliers	0	0
Molprobity Score[f]		1.17 (98th percentile)	1.11 (99th percentile)
Molprobity Clashscore[f]		2.31	2.28

[a] Numbers in parentheses refer to the highest resolution shell.

[b] R_{meas} is the redundancy-independent merging R factor.[73]

[c] R_{pim} is the precision-indicating merging R factor.[73]

[d] Correlation between intensities from random half-sets of data.[74]

[e] R_{free} was calculated using a test set comprising 5% of the data.

[f] Calculated with the program MOLPROBITY.[75]

REFERENCES

1. Mancuso, G.; Midiri, A.; Gerace, E.; Biondo, C., Bacterial antibiotic resistance: the most critical pathogens. *Pathogens* **2021,** *10* (10). DOI: 10.3390/pathogens10101310.

2. Papp-Wallace, K. M.; Endimiani, A.; Taracila, M. A.; Bonomo, R. A., Carbapenems: past, present, and future. *Antimicrob. Agents Chemother.* **2011,** *55* (11), 4943-4960. DOI: 10.1128/aac.00296-11.

3. Bonnin, R. A.; Jousset, A. B.; Emeraud, C.; Oueslati, S.; Dortet, L.; Naas, T., Genetic diversity, biochemical properties, and detection methods of minor carbapenemases in *Enterobacterales*. *Front. Med.* **2020,** *7*, 616490. DOI: 10.3389/fmed.2020.616490.

4. Naas, T.; Dortet, L.; Iorga, B. I., Structural and functional aspects of class A carbapenemases. *Curr. Drug Targets* **2016,** *17* (9), 1006-1028. DOI: 10.2174/1389450117666160310144501.

5. Walther-Rasmussen, J.; Hoiby, N., Class A carbapenemases. *J. Antimicrob. Chemother.* **2007,** *60* (3), 470-482. DOI: 10.1093/jac/dkm226.

6. Poirel, L.; Le Thomas, I.; Naas, T.; Karim, A.; Nordmann, P., Biochemical sequence analyses of GES-1, a novel class A extended-spectrum β-lactamase, and the class 1 integron In52 from *Klebsiella pneumoniae*. *Antimicrob. Agents Chemother.* **2000,** *44* (3), 622-632.

7. Naas, T.; Oueslati, S.; Bonnin, R. A.; Dabos, M. L.; Zavala, A.; Dortet, L.; Retailleau, P.; Iorga, B. I., Beta-lactamase database (BLDB) - structure and function. *J. Enzyme Inhib. Med. Chem.* **2017,** *32* (1), 917-919. DOI: 10.1080/14756366.2017.1344235.

8. Recio, R.; Mancheno, M.; Viedma, E.; Villa, J.; Orellana, M. A.; Lora-Tamayo, J.; Chaves, F., Predictors of mortality in bloodstream infections caused by *Pseudomonas aeruginosa* and impact of antimicrobial resistance and bacterial virulence. *Antimicrob. Agents Chemother.* **2020,** *64* (2). DOI: 10.1128/AAC.01759-19.

9. Cuzon, G.; Bogaerts, P.; Bauraing, C.; Huang, T. D.; Bonnin, R. A.; Glupczynski, Y.; Naas, T., Spread of plasmids carrying multiple GES variants. *Antimicrob. Agents Chemother.* **2016,** *60* (8), 5040-5043. DOI: 10.1128/AAC.00360-16.

10. Polotto, M.; Casella, T.; de Lucca Oliveira, M. G.; Rubio, F. G.; Nogueira, M. L.; de Almeida, M. T.; Nogueira, M. C., Detection of *P. aeruginosa* harboring *bla*CTX-M-2, *bla*GES-1 and *bla*GES-5, *bla*IMP-1 and *bla*SPM-1 causing infections in Brazilian tertiary-care hospital. *BMC Infect. Dis.* **2012,** *12*, 176. DOI: 10.1186/1471-2334-12-176.

11. Barrios, H.; Garza-Ramos, U.; Ochoa-Sanchez, L. E.; Reyna-Flores, F.; Rojas-Moreno, T.; Morfin-Otero, R.; Rodriguez-Noriega, E.; Garza-Gonzalez, E.; Gonzalez, G.; Volkow, P.; Cornejo-Juarez, P.; Red, M. S. G.; Silva-Sanchez, J., A plasmid-encoded class 1 integron contains GES-type extended-spectrum β-lactamases in *Enterobacteriaceae* clinical isolates in Mexico. *Antimicrob. Agents Chemother*. **2012,** *56* (7), 4032-4034. DOI: 10.1128/AAC.05980-11.

12. Khan, A.; Tran, T. T.; Rios, R.; Hanson, B.; Shropshire, W. C.; Sun, Z.; Diaz, L.; Dinh, A. Q.; Wanger, A.; Ostrosky-Zeichner, L.; Palzkill, T.; Arias, C. A.; Miller, W. R., Extensively drug-resistant *Pseudomonas aeruginosa* ST309 harboring tandem Guiana extended spectrum β-lactamase enzymes: a newly emerging threat in the United States. *Open Forum Infect. Dis.* **2019,** *6* (7), ofz273. DOI: 10.1093/ofid/ofz273.

13. Pasteran, F.; Faccone, D.; Petroni, A.; Rapoport, M.; Galas, M.; Vazquez, M.; Procopio, A., Novel variant (*bla*(VIM-11)) of the metallo-β-lactamase *bla*(VIM) family in a GES-1 extended-spectrum-β-lactamase-producing *Pseudomonas aeruginosa* clinical isolate in Argentina. *Antimicrob. Agents Chemother.* **2005,** *49* (1), 474-475. DOI: 10.1128/AAC.49.1.474-475.2005.

14. Charfi-Kessis, K.; Mansour, W.; Ben Haj Khalifa, A.; Mastouri, M.; Nordmann, P.; Aouni, M.; Poirel, L., Multidrug-resistant *Acinetobacter baumannii* strains carrying the *bla*(OxA-23) and the

bla(GES-11) genes in a neonatology center in Tunisia. *Microb. Pathog.* **2014,** *74*, 20-24. DOI: 10.1016/j.micpath.2014.07.003.

15. Drawz, S. M.; Bonomo, R. A., Three decades of β-lactamase inhibitors. *Clin. Microbiol. Rev.* **2010,** *23* (1), 160-201. DOI: 10.1128/CMR.00037-09.

16. Arer, V.; Kar, D., Biochemical exploration of β-lactamase inhibitors. *Front. Genet.* **2022,** *13*, 1060736. DOI: 10.3389/fgene.2022.1060736.

17. Hetzler, L.; Kollef, M. H.; Yuenger, V.; Micek, S. T.; Betthauser, K. D., New antimicrobial treatment options for severe Gram-negative infections. *Curr. Opin. Crit. Care* **2022,** *28* (5), 522-533. DOI: 10.1097/MCC.0000000000000968.

18. Kanj, S. S.; Bassetti, M.; Kiratisin, P.; Rodrigues, C.; Villegas, M. V.; Yu, Y.; van Duin, D., Clinical data from studies involving novel antibiotics to treat multidrug-resistant Gram-negative bacterial infections. *Int. J. Antimicrob. Agents* **2022,** *60* (3), 106633. DOI: 10.1016/j.ijantimicag.2022.106633.

19. Bassetti, M.; Castaldo, N.; Fantin, A.; Giacobbe, D. R.; Vena, A., Antibiotic therapy for nonfermenting Gram-negative bacilli infections: future perspectives. *Curr. Opin. Infec. Dis.* **2023,** *36* (6), 615-622. DOI: 10.1097/QCO.0000000000000984.

20. Butler, M. S.; Henderson, I. R.; Capon, R. J.; Blaskovich, M. A. T., Antibiotics in the clinical pipeline as of December 2022. *J. Antibiot. (Tokyo)* **2023,** *76* (8), 431-473. DOI: 10.1038/s41429-023-00629-8.

21. Onoue, H.; Narukawa, Y., Synthesis and antibacterial activity of 5-methylcarbapenems. *J. Antibiot. (Tokyo)* **1989,** *42* (7), 1100-1113. DOI: 10.7164/antibiotics.42.1100.

22. Awasthi, S.; Gupta, S.; Tripathi, R.; Nair, N. N., Mechanism and kinetics of aztreonam hydrolysis catalyzed by class-C β-lactamase: a temperature-accelerated sliced sampling study. *J. Phys. Chem. B* **2018,** *122* (15), 4299-4308. DOI: 10.1021/acs.jpcb.8b01287.

23. Gupta, R.; Al-Kharji, N.; Alqurafi, M. A.; Nguyen, T. Q.; Chai, W.; Quan, P.; Malhotra, R.; Simcox, B. S.; Mortimer, P.; Brammer Basta, L. A.; Rohde, K. H.; Buynak, J. D., Atypically modified carbapenem antibiotics display improved antimycobacterial activity in the absence of β-lactamase inhibitors. *ACS Infect. Dis.* **2021,** *7* (8), 2425-2436. DOI: 10.1021/acsinfecdis.1c00185.

24. Smith, C. A.; Stewart, N. K.; Toth, M.; Quan, P.; Buynak, J. D.; Vakulenko, S. B., The C5α-methyl-substituted carbapenem NA-1-157 exhibits potent activity against *Klebsiella* spp. isolates producing OXA-48-type carbapenemases. *ACS Infect. Dis.* **2023,** *9* (5), 1123-1136. DOI: 10.1021/acsinfecdis.3c00059.

25. CLSI *Performance standards for antimicrobial susceptibility testing. 33rd ed. CLSI supplement M100.*; Clinical and Laboratory Standards Institute: Wayne, PA, 2023.

26. Eliopoulos, G. M.; Moellering Jr., R. C., Antimicrobial Combinations. In *Antibiotics in Laboratory Medicine*, 4th ed.; Lorian, V., Ed. Williams & Wilkins: Baltimore, MD, 1996.

27. Smith, C. A.; Antunes, N. T.; Stewart, N. K.; Toth, M.; Kumarasiri, M.; Chang, M.; Mobashery, S.; Vakulenko, S. B., Structural basis for carbapenemase activity of the OXA-23 β-lactamase from *Acinetobacter baumannii*. *Chem. Biol.* **2013,** *20* (9), 1107-1115. DOI: 10.1016/j.chembiol.2013.07.015.

28. Frase, H.; Shi, Q.; Testero, S. A.; Mobashery, S.; Vakulenko, S. B., Mechanistic basis for the emergence of catalytic competence against carbapenem antibiotics by the GES family of β-lactamases. *J. Biol. Chem.* **2009,** *284* (43), 29509-29513. DOI: 10.1074/jbc.M109.011262.

29. Stewart, N. K.; Smith, C. A.; Frase, H.; Black, D. J.; Vakulenko, S. B., Kinetic and structural requirements for carbapenemase activity in GES-type β-lactamases. *Biochemistry* **2015,** *54* (2), 588-597. DOI: 10.1021/bi501052t.

30. Cortina, G. A.; Hays, J. M.; Kasson, P. M., Conformational intermediate that controls KPC-2 catalysis and β-lactam drug resistance. *ACS Catal.* **2018,** *8* (4), 2741-2747. DOI: 10.1021/acscatal.7b03832.

31. Stewart, N. K.; Toth, M.; Alqurafi, M. A.; Chai, W.; Nguyen, T. Q.; Quan, P.; Lee, M.; Buynak, J. D.; Smith, C. A.; Vakulenko, S. B., C6 Hydroxymethyl-substituted carbapenem MA-1-206 inhibits the major *Acinetobacter baumannii* carbapenemase OXA-23 by impeding deacylation. *mBio* **2022,** *13* (3), e0036722. DOI: 10.1128/mbio.00367-22.

32. Silverman, R. B., Mechanism-based enzyme inactivators. *Methods Enzymol.* **1995,** *249*, 240-283. DOI: 10.1016/0076-6879(95)49038-8.

33. Copeland, R. A., *Evaluation of enzyme inhibitors in drug discovery: a guide for medicinal chemists and pharmacologists*. second ed.; Wiley-Interscience: Hoboken, NJ, 2013.

34. McWhirter, C., Kinetic mechanisms of covalent inhibition. In *Annu. Rep. Med. Chem.*, Ward, R. A.; Grimster, N. P., Eds. Academic Press: 2021; Vol. 56, pp 1-31. DOI: https://doi.org/10.1016/bs.armc.2020.11.001.

35. Frase, H.; Smith, C. A.; Toth, M.; Champion, M. M.; Mobashery, S.; Vakulenko, S. B., Identification of products of inhibition of GES-2 β-lactamase by tazobactam by X-ray crystallography and spectrometry. *J. Biol. Chem.* **2011,** *286* (16), 14396-14409. DOI: 10.1074/jbc.M110.208744.

36. Frase, H.; Toth, M.; Champion, M. M.; Antunes, N. T.; Vakulenko, S. B., Importance of position 170 in the inhibition of GES-type β-lactamases by clavulanic acid. *Antimicrob. Agents Chemother.* **2011,** *55* (4), 1556-1562. DOI: 10.1128/aac.01292-10.

37. Zandi, T. A.; Townsend, C. A., Competing off-loading mechanisms of meropenem from an L,D-transpeptidase reduce antibiotic effectiveness. *Proc. Natl. Acad. Sci. U. S. A.* **2021,** *118* (27). DOI: 10.1073/pnas.2008610118.

38. Sun, C.; Wu, J.; Pan, Y., Characterization of novel hydrolysis products of carbapenems by electrospray ionization mass spectrometry. *Rapid Commun. Mass Spectrom.* **2009,** *23* (19), 3205-3212. DOI: 10.1002/rcm.4240.

39. Triboulet, S.; Dubee, V.; Lecoq, L.; Bougault, C.; Mainardi, J. L.; Rice, L. B.; Etheve-Quelquejeu, M.; Gutmann, L.; Marie, A.; Dubost, L.; Hugonnet, J. E.; Simorre, J. P.; Arthur, M., Kinetic features of L,D-transpeptidase inactivation critical for β-lactam antibacterial activity. *PloS One* **2013,** *8* (7), e67831. DOI: 10.1371/journal.pone.0067831.

40. Schapira, M.; Totrov, M.; Abagyan, R., Prediction of the binding energy for small molecules, peptides and proteins. *J. Mol. Recognit.* **1999,** *12* (3), 177-190. DOI: 10.1002/(SICI)1099-1352(199905/06)12:3<177::AID-JMR451>3.0.CO;2-Z.

41. Curley, K.; Pratt, R. F., The oxyanion hole in serine β-lactamase catalysis: interactions of thiono substrates with the active site. *Bioorg. Chem.* **2000,** *28* (6), 338-356. DOI: 10.1006/bioo.2000.1184.

42. Galdadas, I.; Qu, S.; Oliveira, A. S. F.; Olehnovics, E.; Mack, A. R.; Mojica, M. F.; Agarwal, P. K.; Tooke, C. L.; Gervasio, F. L.; Spencer, J.; Bonomo, R. A.; Mulholland, A. J.; Haider, S., Allosteric communication in class A β-lactamases occurs via cooperative coupling of loop dynamics. *eLife* **2021,** *10*. DOI: 10.7554/eLife.66567.

43. Papp-Wallace, K. M.; Taracila, M.; Wallace, C. J.; Hujer, K. M.; Bethel, C. R.; Hornick, J. M.; Bonomo, R. A., Elucidating the role of Trp105 in the KPC-2 β-lactamase. *Protein Sci.* **2010,** *19* (9), 1714-1727. DOI: 10.1002/pro.454.

44. Doucet, N.; De Wals, P. Y.; Pelletier, J. N., Site-saturation mutagenesis of Tyr-105 reveals its importance in substrate stabilization and discrimination in TEM-1 β-lactamase. *J. Biol. Chem.* **2004,** *279* (44), 46295-46303. DOI: 10.1074/jbc.M407606200.

45. De Wals, P. Y.; Doucet, N.; Pelletier, J. N., High tolerance to simultaneous active-site mutations in TEM-1 β-lactamase: Distinct mutational paths provide more generalized β-lactam recognition. *Protein Sci.* **2009,** *18* (1), 147-160. DOI: 10.1002/pro.25.

46. Majiduddin, F. K.; Palzkill, T., Amino acid residues that contribute to substrate specificity of class A β-lactamase SME-1. *Antimicrob. Agents Chemother.* **2005,** *49* (8), 3421-3427. DOI: 10.1128/AAC.49.8.3421-3427.2005.

47. Patel, M. P.; Hu, L.; Brown, C. A.; Sun, Z.; Adamski, C. J.; Stojanoski, V.; Sankaran, B.; Prasad, B. V. V.; Palzkill, T., Synergistic effects of functionally distinct substitutions in β-lactamase variants shed light on the evolution of bacterial drug resistance. *J. Biol. Chem.* **2018,** *293* (46), 17971-17984. DOI: 10.1074/jbc.RA118.003792.

48. Ke, W.; Bethel, C. R.; Papp-Wallace, K. M.; Pagadala, S. R.; Nottingham, M.; Fernandez, D.; Buynak, J. D.; Bonomo, R. A.; van den Akker, F., Crystal structures of KPC-2 β-lactamase in complex with 3-nitrophenyl boronic acid and the penam sulfone PSR-3-226. *Antimicrob. Agents Chemother.* **2012,** *56* (5), 2713-2718. DOI: 10.1128/AAC.06099-11.

49. Bethel, C. R.; Hujer, A. M.; Hujer, K. M.; Thomson, J. M.; Ruszczycky, M. W.; Anderson, V. E.; Pusztai-Carey, M.; Taracila, M.; Helfand, M. S.; Bonomo, R. A., Role of Asp104 in the SHV β-lactamase. *Antimicrob. Agents Chemother.* **2006,** *50* (12), 4124-4131. DOI: 10.1128/AAC.00848-06.

50. Lovell, S. C.; Word, J. M.; Richardson, J. S.; Richardson, D. C., The penultimate rotamer library. *Proteins* **2000,** *40* (3), 389-408.

51. Smith, C. A.; Frase, H.; Toth, M.; Kumarasiri, M.; Wiafe, K.; Munoz, J.; Mobashery, S.; Vakulenko, S. B., Structural basis for progression toward the carbapenemase activity in the GES family of β-lactamases. *J. Am. Chem. Soc.* **2012,** *134* (48), 19512-19515. DOI: 10.1021/ja308197j.

52. Bondi, A., van der Waals volumes and radii. *J. Phys. Chem.* **1964,** *68* (3), 441-451. DOI: 10.1021/j100785a001.

53. CLSI *Methods for dilution antimicrobial susceptibility tests for bacteria that grow aerobically; Approved standard-11th edition. CLSI document M07-A11.*; Clinical and Laboratory Standards Institute: Wayne, PA, 2018.

54. Odds, F. C., Synergy, antagonism, and what the chequerboard puts between them. *J. Antimicrob. Chemother.* **2003,** *52* (1), 1. DOI: 10.1093/jac/dkg301.

55. Copeland, R. A.; Basavapathruni, A.; Moyer, M.; Scott, M. P., Impact of enzyme concentration and residence time on apparent activity recovery in jump dilution analysis. *Anal. Biochem.* **2011,** *416* (2), 206-210. DOI: 10.1016/j.ab.2011.05.029.

56. Kabsch, W., XDS. *Acta Crystallogr. Sect. D: Biol. Crystallogr.* **2010,** *66* (Pt 2), 125-132. DOI: 10.1107/s0907444909047337.

57. Evans, P. R.; Murshudov, G. N., How good are my data and what is the resolution? *Acta Crystallogr. Sect. D: Biol. Crystallogr.* **2013,** *69* (Pt 7), 1204-1214. DOI: 10.1107/s0907444913000061.

58. Vonrhein, C.; Flensburg, C.; Keller, P.; Sharff, A.; Smart, O.; Paciorek, W.; Womack, T.; Bricogne, G., Data processing and analysis with the autoPROC toolbox. *Acta Crystallogr. Sect. D: Biol. Crystallogr.* **2011,** *67* (Pt 4), 293-302. DOI: 10.1107/S0907444911007773.

59. Afonine, P. V.; Grosse-Kunstleve, R. W.; Echols, N.; Headd, J. J.; Moriarty, N. W.; Mustyakimov, M.; Terwilliger, T. C.; Urzhumtsev, A.; Zwart, P. H.; Adams, P. D., Towards automated

crystallographic structure refinement with phenix.refine. *Acta Crystallogr. Sect. D: Biol. Crystallogr.* **2012,** *68* (Pt 4), 352-67. DOI: 10.1107/S0907444912001308.

60. Emsley, P.; Cowtan, K., Coot: model-building tools for molecular graphics. *Acta Crystallogr. Sect. D: Biol. Crystallogr.* **2004,** *60* (Pt 12 Pt 1), 2126-2132. DOI: 10.1107/s0907444904019158.

61. Abagyan, R.; Totrov, M., Biased probability Monte Carlo conformational searches and electrostatic calculations for peptides and proteins. *J. Mol. Biol.* **1994,** *235* (3), 983-1002. DOI: 10.1006/jmbi.1994.1052.

62. Abagyan, R.; Totrov, M.; Kuznetsov, D., ICM—A new method for protein modeling and design: Applications to docking and structure prediction from the distorted native conformation. *J. Comput. Chem.* **1994,** *15* (5), 488-506. DOI: https://doi.org/10.1002/jcc.540150503.

63. Roos, K.; Wu, C.; Damm, W.; Reboul, M.; Stevenson, J. M.; Lu, C.; Dahlgren, M. K.; Mondal, S.; Chen, W.; Wang, L.; Abel, R.; Friesner, R. A.; Harder, E. D., OPLS3e: Extending force field coverage for drug-like small molecules. *J. Chem. Theory Comput.* **2019,** *15* (3), 1863-1874. DOI: 10.1021/acs.jctc.8b01026.

64. Jorgensen, W. L.; Chandrasekhar, J.; Madura, J. D.; Impey, R. W.; Klein, M. L., Comparison of simple potential functions for simulating liquid water. *J. Chem. Phys.* **1983,** *79*, 926-935. DOI: https://doi.org/10.1063/1.445869.

65. Martyna, G. J.; Klein, M. L.; Tuckerman, M., Nosé–Hoover chains: The canonical ensemble via continuous dynamics. *J. Chem. Phys.* **1992,** *97* (4), 2635-2643. DOI: 10.1063/1.463940.

66. Bowers, K. J.; Chow, E.; Xu, H.; Dror, R. O.; Eastwood, M. P.; Gregersen, B. A.; Klepeis, J. L.; Kolossvary, I.; Moraes, M. A.; Sacerdoti, F. D.; Salmon, J. K.; Shan, Y.; Shaw, D. E., Scalable algorithms for molecular dynamics simulations on commodity clusters. In *ACM/IEEE Conference on Supercomputing (SC06)*, Tampa, FL, 2006.

67. Olsson, M. H.; Sondergaard, C. R.; Rostkowski, M.; Jensen, J. H., PROPKA3: consistent treatment of internal and surface residues in empirical pKa predictions. *J. Chem. Theory Comput.* **2011,** *7* (2), 525-537. DOI: 10.1021/ct100578z.

68. Hornak, V.; Abel, R.; Okur, A.; Strockbine, B.; Roitberg, A.; Simmerling, C., Comparison of multiple Amber force fields and development of improved protein backbone parameters. *Proteins* **2006,** *65* (3), 712-725. DOI: 10.1002/prot.21123.

69. Wang, J.; Wolf, R. M.; Caldwell, J. W.; Kollman, P. A.; Case, D. A., Development and testing of a general amber force field. *J. Comput. Chem.* **2004,** *25* (9), 1157-1174. DOI: 10.1002/jcc.20035.

70. Vanquelef, E.; Simon, S.; Marquant, G.; Garcia, E.; Klimerak, G.; Delepine, J. C.; Cieplak, P.; Dupradeau, F. Y., R.E.D. Server: a web service for deriving RESP and ESP charges and building force field libraries for new molecules and molecular fragments. *Nucleic Acids Res.* **2011,** *39* (Web Server issue), W511-7. DOI: 10.1093/nar/gkr288.

71. Case, D. A.; Belfon, K.; Ben-Shalom, I. Y.; Brozell, S. R.; Cerutti, D. S.; Cheatham, I., T.E. ; Cruzeiro, V. W. D.; Darden, T. A.; Duke, R. E.; Giambasu, G.; Gilson, M. K.; Gohlke, H.; Goetz, A. W.; Harris, R.; Izadi, S.; Izmailov, S. A.; Kasavajhala, K.; Kovalenko, A.; Krasny, R.; Kurtzman, T.; Lee, T. S.; LeGrand, S.; Li, P.; Lin, C.; Liu, J.; Luchko, T.; Luo, R.; Man, V.; Merz, K. M.; Miao, Y.; Mikhailovskii, O.; Monard, G.; Nguyen, H.; Onufriev, A.; Pan, F.; Pantano, S.; Qi, R.; Roe, D. R.; Roitberg, A.; Sagui, C.; Schott-Verdugo, S.; Shen, J.; Simmerling, C. L.; Skrynnikov, N. R.; Smith, J.; Swails, J.; Walker, R. C.; Wang, J.; Wilson, L.; Wolf, R. M.; Wu, X.; Xiong, Y.; Xue, Y.; York, D. M.; Kollman, P. A. *AMBER 2020*; University of California: San Francisco, 2020.

72. Grossfield, A. *WHAM: an implementation of the weighted histogram analysis method*; 2013.

73. Weiss, M. S., Global indicators of X-ray data quality. *J. Appl. Crystallogr.* **2001,** *34* (2), 130-135. DOI: 10.1107/S0021889800018227.

74. Karplus, P. A.; Diederichs, K., Linking crystallographic model and data quality. *Science* **2012,** *336* (6084), 1030-1033. DOI: 10.1126/science.1218231.

75. Chen, V. B.; Arendall, W. B., 3rd; Headd, J. J.; Keedy, D. A.; Immormino, R. M.; Kapral, G. J.; Murray, L. W.; Richardson, J. S.; Richardson, D. C., MolProbity: all-atom structure validation for macromolecular crystallography. *Acta Crystallogr. Sect. D: Biol. Crystallogr.* **2010,** *66* (Pt 1), 12-21. DOI: 10.1107/S0907444909042073.

TOC Graphic